Master's Thesis

A Study on Adhesive Strength of Co-Cured CFRP-Metal Multi-Material Joints and Joint Failure Detection Using Electrical Resistance Measurement

Ho-Min Lee

Department of Mechanical Engineering

Graduate School of UNIST

2017

A Study on Adhesive Strength of Co-Cured CFRP-Metal Multi-Material Joints and Joint Failure Detection Using Electrical Resistance Measurement

Ho-Min Lee

Department of Mechanical Engineering

Graduate School of UNIST

A Study on Adhesive Strength of Co-Cured CFRP-Metal Multi-Material Joints and Joint Failure Detection Using Electrical Resistance Measurement

A thesis
submitted to the Graduate School of UNIST
in partial fulfillment of the
requirements for the degree of
Master of Science

Ho-Min Lee

6. 12. 2017
Approved by

_____
Advisor
Young-Bin Park

A Study on Adhesive Strength of Co-Cured CFRP-Metal Multi-Material Joints and Joint Failure Detection Using Electrical Resistance Measurement

Ho-Min Lee

This certifies that the thesis of Ho-Min Lee is approved.

6. 12. 2017

signature

_____

Advisor: Young-Bin Park

signature

_____

Hyung Wook Park

signature

_____

Wooseok Ji

Abstract

Carbon-Fiber-Reinforced Plastics (CFRPs) are composite materials, consisting of carbon fibers and polymeric matrices. Depending on the types of carbon fiber and polymer used, CFRP can have a variety of properties. Generally, CFRP show high specific strength and stiffness, so it is regarded as a substitute material for existing structural materials, such as metals. In addition, CFRP can have high temperature or corrosion resistance based on the type of matrix used. For this reason, despite the high price of carbon fiber, it is widely applied to the aerospace industry and has gradually expanded into the automotive industry in recent years.

Despite their advantages in terms of weigh-saving, it is not possible to replace all the metal parts, especially ultra-high-strength steels, *etc*., with CFRPs due to their limitations in intrinsic properties. This has led to the "multi-material design" concept, in which hetero-junctions between composites and metals have become an important issue. Typical methods for multi-material joining include mechanical joining and adhesive bonding. Mechanical joining, *e.g.*, riveting, mechanical fastening, *etc*., leads to high stress concentration due to the pre-drilled holes, and it has to bear additional weight of inserts, such as bolts and rivets. Adhesive bonding, on the other hand, requires time of adhesive curing in addition to matrix curing, which has detrimental effects on manufacturing time and costs. To overcome these drawbacks, the co-curing method, in which the infused resin serves as the adhesive and therefore, the additional adhesive curing time can be omitted, has been considered as an alternative cost-effective adhesive joining method.

Although multi-material joining using the co-curing method results in a lower adhesive strength than adhesive-bonded joints, this method can reduce the curing time since adhesive and CFRP curing proceed simultaneously and makes possible real-time health monitoring of the joints using electrical resistance measurement because carbon fiber directly contacts the metal surface, both of which are electrically conductive.

In this study, we showed that structural health monitoring using electrical resistance measurement at the junction between metals and CFRPs joined by co-curing is feasible, and its effectiveness was studied as compared to the case where a conductive epoxy was used as the adhesive. Also, we measured the adhesive strength and determined the possibility of failure detection when a steel bushing, which is one of metal inserts, was joined by co-curing with CFRP. In addition, the interfacial strength between metal and polymer resin was enhanced by atmospheric plasma surface treatment since aluminum-CFRP co-cured joints initially had poor lap shear strength.

CFRP was fabricated by plain-woven carbon fibers and unsaturated polyester resin, and stainless steel and aluminum sheets were used as the metals for multi-material joining. To detect the failure at the junction between CFRP and metal, co-curing was adopted rather than an epoxy adhesive containing dispersed carbon nanotubes (CNTs).

In the co-curing process, conductive carbon fiber and metals directly contacted each other, so electric current can flow through both materials. As the initial load increased, the resistance gradually decreased, and then increased drastically due to de-bonding at the co-cured joints. Electrical resistance was increased when the contact area between carbon fiber and metal surface were decreased, so it can monitor the failure detection at the multi-material joints. Single-lap shear test was performed for each joint, and four-wire Kelvin resistance measurement was adopted to measure the change in resistance during the test.

To apply this research, we manufactured steel bushing-inserted CFRPs joined by co-curing method. Push-out tests were performed to measure the adhesive strength between the inserts and CFRPs. Next, we demonstrated the proof-of-concept of health monitoring at the co-cured joints between steel bushings and CFRPs using electrical resistance measurements.

In the case of aluminum-CFRP co-cured joints, the adhesive strength was about 30% compared to the other joints, so we applied atmospheric plasma to the metal surfaces such as steel, aluminum and steel bushings. Upon plasma treatment, the adhesive strength of aluminum-CFRPs co-cured joint was increased by 300%. After plasma treatment, the number of hydrogen bonds increased between the unsaturated polyester and the metal surfaces as the metal surfaces were getting more hydrophilic. Wettability was increased due to the increase of -OH functional groups on the metal surfaces, which led to the enhancement of the interfacial adhesive strength between polyester and metal surfaces bonded through the co-curing process. As the adhesive strength increased with plasma treatment, it was shown that the gradient of the resistance rate decreases prior to the complete destruction at the joints. For this reason, it is important to identify the optimized point to secure failure strength and predict joint failure.

Based on the experimental results, it is feasible to monitor failures in multi-material joints between CFRPs and conductive metals real-time by measuring the change in resistance. This ensures the safety of various CFRP-metal multi-material structures, including aircraft, automotive parts, civil structures, sporting goods, electronic modules, and biomedical devices.

Contents

List of Figures

List of Tables

1. Introduction

Since 2015, regulations on environmental pollution in each country have become stricter and stricter. The United States, Japan and China are regulating fuel economy and Europe is regulating greenhouse gas emissions. As a result, research has been actively conducted to improve fuel efficiency in the automobile industry. Methods to improve fuel economy include power train improvement, resistance reduction design, vehicle weight reduction and alternative energy technology. Among them, improvement of power train contributes most to improvement of fuel efficiency, but it is difficult to cope with regulations because the technology level is considerably mature and production cycle is too long, so the effect of investment is decreasing. In addition, driving technology using alternative energy has a limit of technological development, and it takes a long time to construct infrastructure at a high cost. Therefore, improvement of fuel efficiency through reduction of vehicle weight is drawing attention as the most realistic and effective method because its development period is relatively short, automotive parts can be lightweighted by various methods. Also, it has the effect of increasing car acceleration, reducing braking distance and increasing steering performance.

When the weight of the car body is reduced by 10 kg, fuel consumption is reduced by 2.8%, and carbon dioxide and nitrogen oxide emissions are reduced by 4.5% and 8.8%, respectively, to meet fuel efficiency regulations and greenhouse gas emission regulations. However, in reality, the weight of car is gradually increasing due to the increase of safety and convenience of consumers. Also, electric cars are attracting attention as a future type of automobile, but the weight of the electric vehicles is increased due to the parts heavier than conventional engines such as electric motors, batteries and fuel cells.

Therefore, in the automobile industry, weight reduction of materials having the largest effect of weight reduction among the light-weighting of structures, manufacturing and materials have attracted attention. The weight reduction of the material refers to a method of completely replacing the existing steel material or partially reducing the weight by combining with other materials. Among them, material change using carbon-fiber-reinforced plastic (CFRP) is receiving the most attention. The CFRP is superior in specific strength and specific stiffness compared to conventional steel, and the weight can be greatly reduced when the body is made of CFRP. However, CFRP is not as good for forming and machining as metal, so there is an obvious limiting factor to the existing composite processing technologies when attempting to replace all parts of automobile. Therefore, steel material is partially replaced rather than completely replaced, hence multi-material joining is essential.

Typical multi-material joining methods include mechanical fastening and adhesive bonding. Laser-assisted metal and plastic (LAMP) [1, 2], self-piercing riveting (SPR) [3], friction stir welding (FSW) [4-6], mechanical clinching [7-10], ultrasonic welding [11, 12] and adhesive bonding [13], as shown in Fig. 1. Among them, SPR, MC methods do not require pre-drilling. In addition, much research has been done due to their simplicity, robustness, low cost, and high productivity. However, they result in high stress concentrations and damage the composite, so they are used only in limited cases. FSW is one of the methods of combined thermos mechanical process. It is possible to join carbon-fiber-reinforced thermoplastic and metal. The disadvantages of this method are the poor surface finish of the welded points and the development of high loads during the joining process. In particular, it cannot be used for thermosetting matrices. In the other two cases, ultrasonic welding and LAMP are joined using high temperature, so they can only be used with thermoplastic polymers. The thermosetting plastic can be joined, if a thermoplastic film is inserted in between. Among them, the bonding using the adhesive does not cause the deterioration of the joint due to heat because the bonding temperature is not high, and it is possible to obtain the high rigidity of the joint due to the face joint and to secure the airtightness of the joint, but requires additional curing time. Also, the surface of polymer or FRP materials should be considered for the joining.
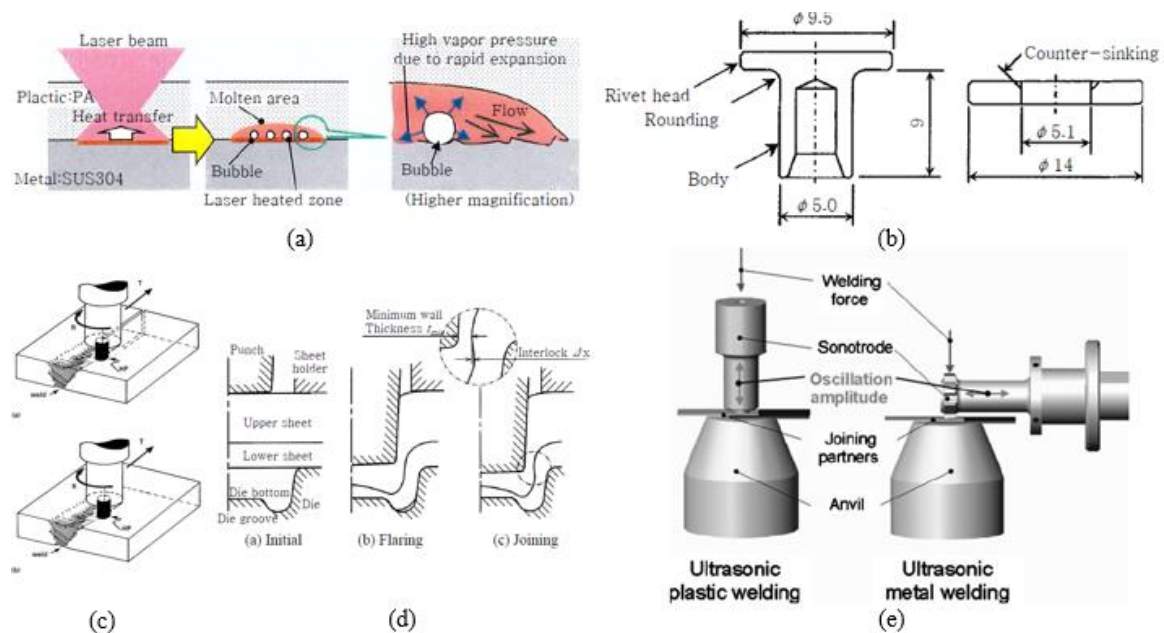
Figure 1. Several methods of the multi-material joining; (a) Plastic induced by bubble in LAMP from [2], (b) SPR body and supporting plate shape [3], (c) Schematic arrangements illustrating FSW in thin plate [6], (d) MC procedure [10] and (e) Schematic of ultrasonic welding [11].

Co-cured joints are considered as multi-material joints between metal and FRP formed using an excess resin of FRP as an adhesive [14-19]. This method requires considering of bonding with metal surface since the adhesive and FRP adherend are the same. In addition, curing and joining can be done simultaneously, thus it can reduce manufacturing time and cost.

In addition, the bonding between different materials greatly depends on the bonding structure, and the collision-absorbing ability may be deteriorated due to the separation during the collision. Therefore, studies are being conducted to structural health monitoring (SHM) of the joints for the safety of driver. There are some researches for the SHM of multi-material joints: eddy current testing, microwave and X-rays, electromagnetic non-destructive evaluation (NDE) systems and electrical resistance.

Among them, the method using electrical resistance, unlike other NDE systems, does not require any special device for measurement and can monitor in real-time. Therefore, Kang *et al.* [20] conducted a research for SHM of multi-material joints using electric resistance. In this paper, the fatigue strength was increased by 12.8% by mixing 2% of carbon nanotubes to the epoxy adhesive, and the breakage of the joint was diagnosed through the change of electrical resistance. However, in Kang's study, it is necessary to mix carbon nanotubes (CNTs) in the adhesive, an additional process is required and the process is complicated for bonding for 80 to 120 minutes, resulting in a decrease in static strength.

In this research, we studied that failure detection of multi-material joints via electrical resistance monitoring without adversely affecting or adding an additional step to the existing manufacturing process. We overcame the problems of conventional research by using co-curing to join dissimilar materials simultaneously as CFRPs are cured. When using co-curing for multi-material joining, the carbon fibers are in direct contact with the metal at the joints, as in Fig. 2, so current can flow between the two materials. Thus, there is no need for a bonding process as compared to the use of an epoxy adhesive and no additional process is required to mix the CNTs for SHM. Also, the phenomenon that the static strength decreases at the joining stage can be prevented. When bonding metal and CFRP using co-curing, it is possible to detect the initiation and propagation of cracks, and it is also possible to diagnose the complete separation at the joint.

3
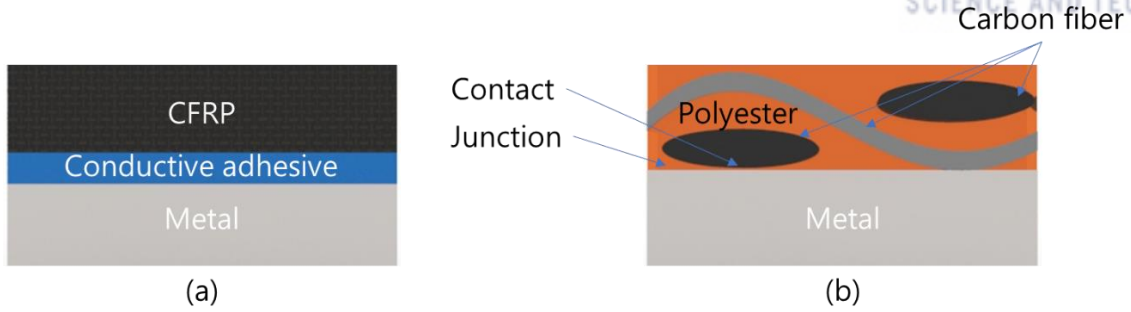
Figure 2. Schematic of the cross-section area at the joints; (a) Conductive adhesive and (b) Co-curing.

In this research, we focused on multi-material joints formed between plain-woven CFRP and metals, such as steel and aluminum, which are often used as structural materials in an automobile. In order to make the current flow through the joints, the co-curing method and the conductive adhesive were used, and the resistances were measured by the 4-probe measurement method. First, we confirmed the possibility of failure detection by measuring the electrical resistance change. Next, metal surface treatment was performed through atmospheric-pressure plasma treatment to improve the adhesive strength. We investigated the underlying mechanism of resistance change in each case and the reason why adhesive strength was improved through plasma treatment.

2. Literature Review

2.1.   Structural Health Monitoring of CFRPs

SHM has two types method such as a schedule-based and real-time monitoring method called NDE. The first of the SHM is eddy current [21-24], which makes it possible to identify microcracks inside the composite that cannot be seen by the naked eye. This method is based on Faraday's law that the shape changes when a loop meets an internal microcrack. However, this method is not suitable for identifying large structures. The measurement equipment was shown in Fig. 3 (b).

The second method is ultrasonic inspection. It identifies the reflected signal when an ultrasonic energy pulse is shot into the structure, which is called C-scan in Fig. (a). The size and position of the internal damage are displayed on the 2D screen [25-27]. These two methods are schedule-based inspection. The limitation of schedule-based inspection is that there is time, labor, and blind spot for inspection.

Real-time inspection includes a fiber Bragg grating (FBG) sensor that passes wavelengths through the optical fiber. When deformation occurs, special wavelengths are reflected. The procedure of this method is shown at Fig. 3 (c). This technique has very fast response and sensitivity, up to 2 nm [28-32]. This method has limitations due to high cost and laborious installment. Especially optical fiber is made of glass and fragile easily occurs.

These three methods are applicable to all FRP materials. CFRP has conductivity different from other FRPs, and it can detect the internal change in real time by measuring the electrical resistance change. In particular, CFRP has advantages over existing structural materials in some respects [33-35], and several studies have been conducted on inspection using electrical resistance change.
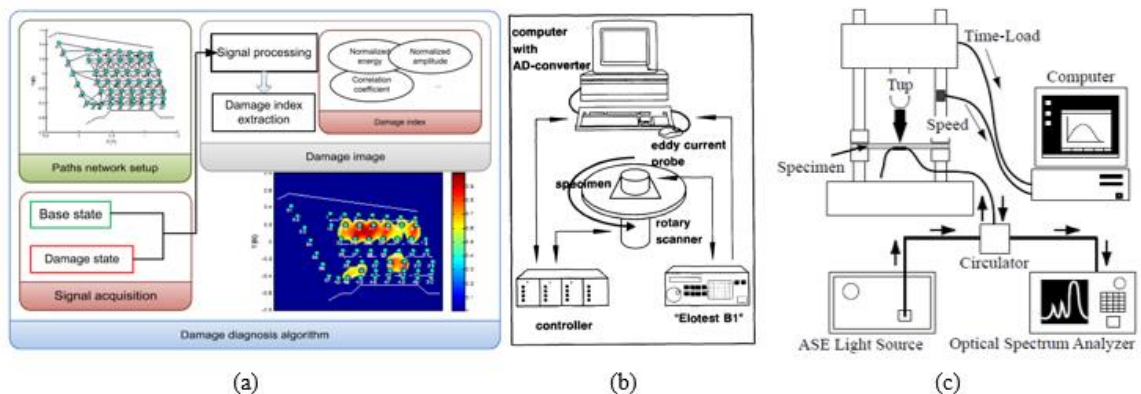
Figure 3. (a) C-scan operation [25], (b) Measurement equipment of eddy-current [21] and (c) Monitoring of reflection spectrum of FBG [28].

D.D.L. Chung *et al.* investigated the piezo-resistivity of unidirectional (UD) CFRPs under cyclic tensile test [36]. He measured resistance by 2 and 4 probes method and compared the piezo-resistivity and contact resistance of the composite. In addition, the piezo-resistivity of UD CFRPs was decreased under tensile loading conditions due to the increased degree of fiber alignment.

In-situ self-sensing CFRPs have been studied more extensively [37-40]. S. Wang *et al.* [37] conducted some tests related with temperature, humidity, mechanical stress and strain. He investigated that the self-sensing mechanism as a sensor of analyzing the piezo-resistivity of carbon fiber interlaminar interface. The specialty of this paper is to take into account the interlaminar behavior of the piezo-resistive material.

In addition, A. Todoroki *et al.* [41, 42] focused on the structural numerical analysis of UD CFRPs and electrical resistance change. The piezo-resistivity in different loading and measurement directions appear in the fabric alignment as shown in Fig. 4 (a). And positive piezo-resistivity was measured in multiaxial loading with poor electrode contact as shown in Fig. 4 (b). This anisometric piezo-resistivity analysis has developed in 2011 with the laminate theory and FEM analysis [43].
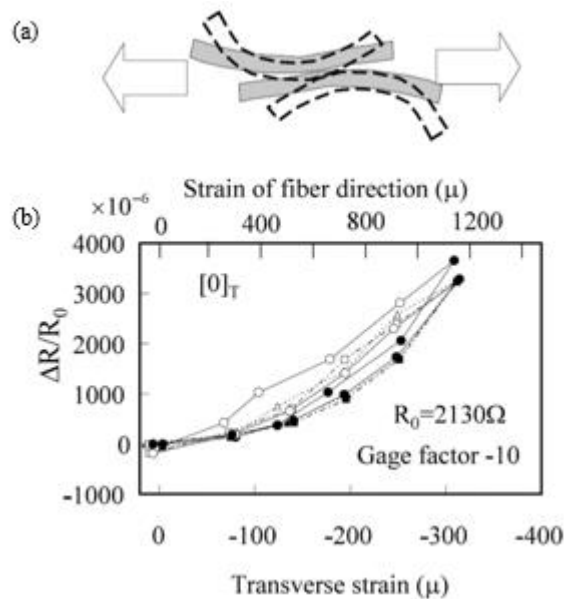
Figure 4. (a) Fiber alignment during the tensile loading and (b) Positive piezo-resistivity during the tensile loading from [42].

He did research on electrode connections with J. Yoshida [44]. A poor electrode connection was claimed to lead to negative piezo-resistivity due to electrical contact damage. Therefore, the electrical resistance change was measured according to the electrode condition of single ply CFRP. He also investigated the poor contact between the composite and the electrodes by FEM analysis.

2.2. Joining Method for CFRPs

The CFRP-metal multi-material joining methods include mechanical fastening and adhesive bonding. Mechanical fastening typically includes screws or rivets with additional components. They generally require predrilled holes in the material for joining. Therefore, mechanical fastening using screws or rivets has a great effect on the joining time. To solve this problem, self-pierce riveting (SPR) [3] and mechanical clinching (MC) [7-10] have been studied. SPR is an improved method to prevent peeling damage in the CFRP part. Fig. 1 (b) shows the body of the SPR developed for CFRP joining and the backing metal to prevent peeling damage of CFRP. To prevent peeling damage from around the hole, it is designed to insert the rivet by putting the base metal at bottom surface of CFRP to be joined.

Fig. 1 (d) shows the multi-material joining by MC. The joined plate, which is overlapped with the upper plate and the lower plate, expands under the lower plate by a punch and extends radially while contacting the bottom of the die. Interlocking is formed and the joining is completed.

These are intuitive in joining and have been studied extensively for their simplicity, robustness, low cost and high productivity. However, they are spot joints that cause high stress concentration, damage the composite and require access from both sides of the joint.

On the other hand, adhesive bonding can join different kinds of materials, hardly deforms by heat, and high stiffness of joints can be obtained due to face to face bonding. However, adhesive bonding has to take into account the surface of all the different materials, and requires additional curing time of the adhesive after curing of the composite which consumes a lot of time. Experimental techniques are also required for uniform thickness and uniform application. Therefore, co-curing which is considered as an adhesively bonded joining method are considered. Research on co-curing has continued [14-19]. The difference the manufacturing process was shown in Fig. 5 (a) and (b).
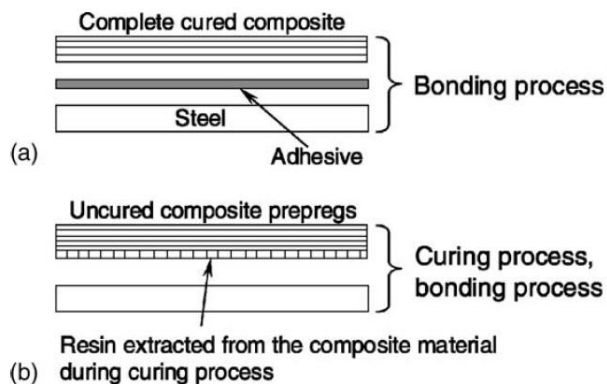
Figure 5. Comparison of the manufacturing process; (a) Adhesively bonded joints and (b) Co-cured joints from [16].

Co-cured joining methods have advantages over adhesive bonded joining due to a simple manufacturing process. In particular, no surface treatment for the composite adherend is required since co-curing uses excess resin from the composite for the adhesive during the manufacturing. For this reason, analysis and design of co-cured joints are simpler than adhesively bonded joints.

Shin *et al.* [16] investigated the process of co-cured single and double lap joints and the properties of co-cured joints. In this research, abrasive surface treatment using a sand-paper was adopted as surface treatment of metal before co-curing. The resin is cured in an autoclave to form a 10 μm thick layer between FRP and metal. Tensile test results show that the co-cured single-lap joint has a bearing capacity of about 5000 N, and the initial failure mechanism causes interfacial failure between steel and composite adherend. Also, the effect of surface roughness was not significant.

2.3.   Stress and Bending Moment Analysis of Single-Lap Shear

Shin *et al.* [16] performed finite element analysis to investigate the behavior of co-cured single-lap joints under tensile loading. In this experiment, the analysis of residual thermal stresses is important because the co-cured single-lap joints pass through the process of falling from 120 to 20 degrees during curing. Thus, ABAQUS 5.8, commercial finite element analysis software [45]. Fig. 6 (a) and (b) show the tensile and shear stresses in the out-of-plane direction of a single-lap joint at the first ply of the composite adherend. These results show that tensile and shear stresses in the out-of-plane direction can fully affect the initial cracks. In addition, when the thermal load graph is checked, it is considered that compression is at x = 0 and tension is added at x = L, so that x = L is more important than x = 0 when tensile load is applied.
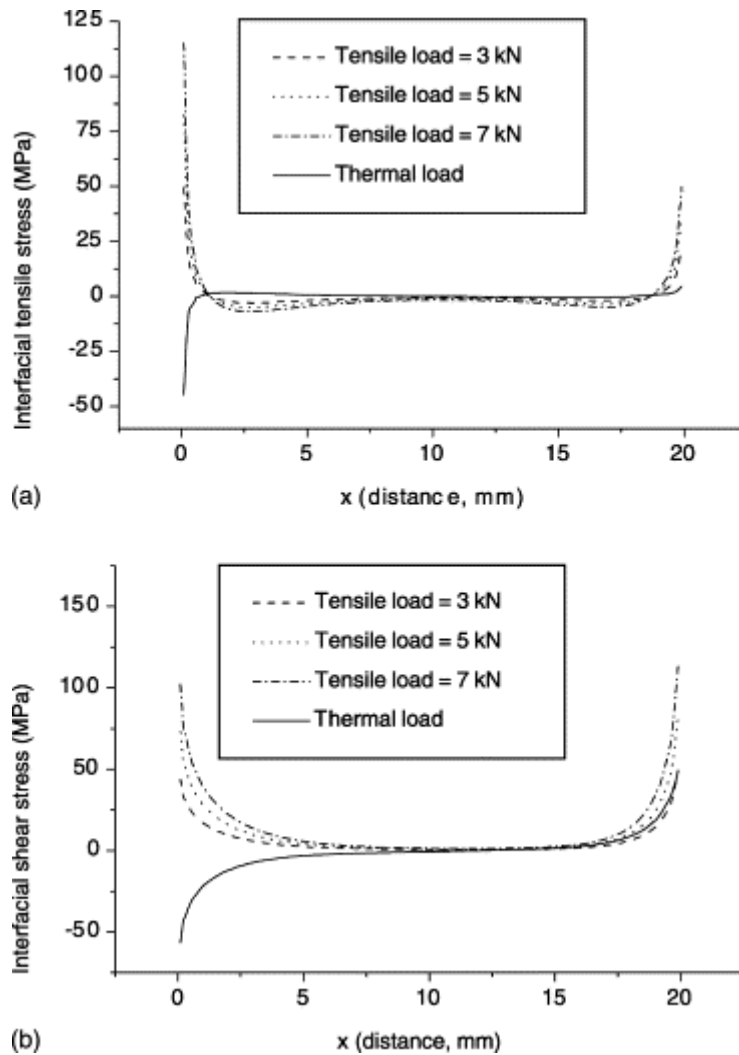
Figure 6. Stress distributions in the co-cured single-lap joint; (a) Out of plane tensile stress distribution and (b) Out of plane shear stress distribution from [16].

2.4.   Surface Treatment for Metal

Adhesive bonding requires design depending on the surface condition and type of base material. For this purpose, surface treatment of materials which want to joining is important. The wetting phenomenon of the adhesive and the surface of the base material greatly affects the adhesive strength, which requires increasing the surface energy of the base material or reducing the surface tension of the adhesive. Common surface treatment processes include cleaning to remove foreign substances and oil, polishing to remove oxide film, chemical treatment to improve affinity and removal of foreign matter and primer treatment to improve the affinity of the surface by applying a primer. Adhesive strength can be increased through these methods.

Atmospheric Plasma Treatment (APT) has increased usage because of low price and flexibility of a continuous process. Low pressure plasma is expensive, heavy maintenance and limited treatment size (by vacuum chamber size). Contrastively, APT solves the vacuum process and it has a low working temperature and a high density of reacting with charged particles [46].

Plasma treatments have hydrophilic or hydrophobic surface properties and alter the surface of metals, plastics, glasses, polymers, and so on. This enhances the adhesion properties and allows bonding of different kinds of materials.

Kim *et al.* [46], used plasma with 10 kV output frequency at the frequency of 16-20 kHz and 10 mm nozzle diameter. The used reaction gas was pure gas in which nitrogen and oxygen were mixed in a ratio of 4: 1.

In this study, contact angle was measured to confirm the degree of hydrophilicity by plasma treatment with different nozzle velocity and nozzle to surface gap, as shown in Fig. 7 (a) and (b), respectively. As the nozzle velocity and gap increased, the contact angle tended to increase. Figure 7 (c) shows the contact angle image before and after plasma treatment.
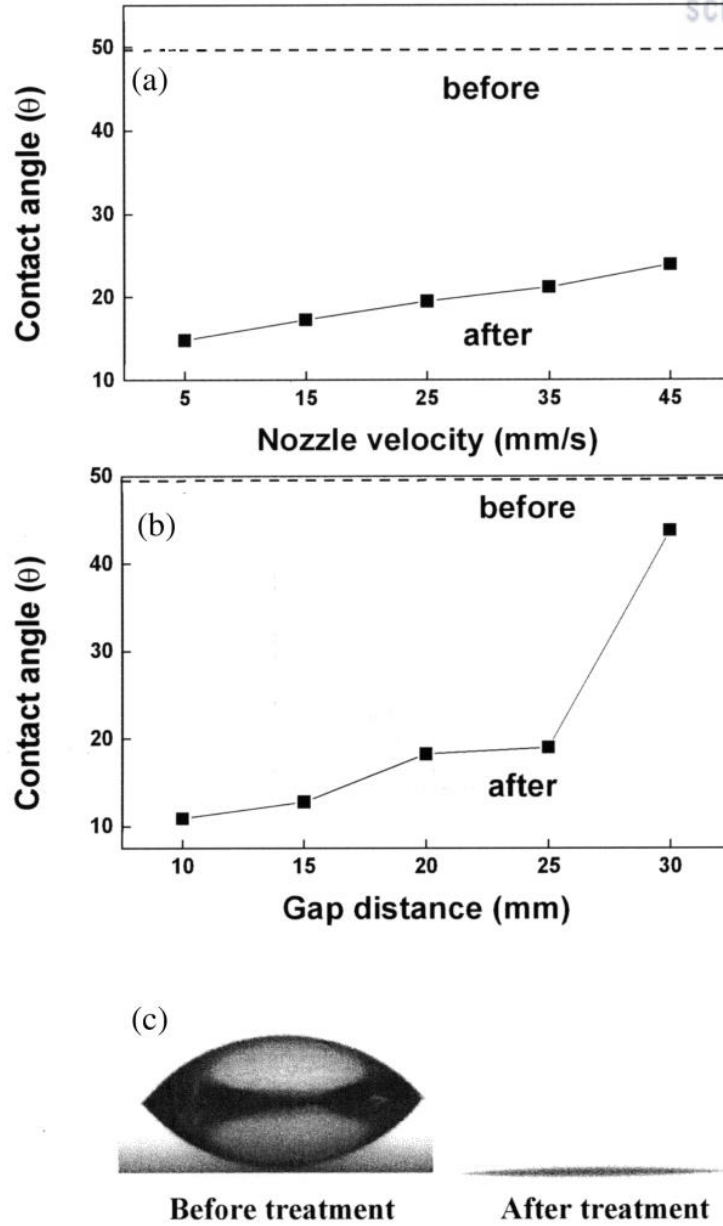
Figure 7. Contact angle under different (a) plasma nozzle velocity and (b) gap distance. (c) Contact angle images before and after plasma treatment in the 5 mm gap distance and 10 mm/s nozzle velocity from [46].

2.5.   Detection of Joint Failures

In general, joints are more prone to fail when static and dynamic loads are applied continuously. Particularly, joining of FRP and metal is difficult because the other materials is bonded. Therefore, in-situ failure detection or damage monitoring in joints has been studied [20, 47-49].

Murayama *et al.* [47] studied the SHM of a huge composite structure using fiber-optic distributed sensors as shown in Fig. 8 (a). Fiber-optic sensors were used to measure the stiffness of the structure and applied to Brillouin Optical Time Domain Reflectometry (BOTDR). In this paper, he used this sensing system to detect the unusual deformation of the adhesive joint of the mast supporting hull and the bulk head.

Kang *et al.* [20] used the electrical resistance to diagnose the multi-material joints as shown in Fig. 8 (b). 2wt% of CNTs were added to the epoxy adhesive, which increased the fatigue strength by 12.8% and the damage of the joint was monitored by measuring the change in electrical resistance. However, this method requires an additional process to mix the CNTs in the adhesive and requires curing at 80°C for 120 minutes to bond, complicating the process and consequently decreasing the static strength.
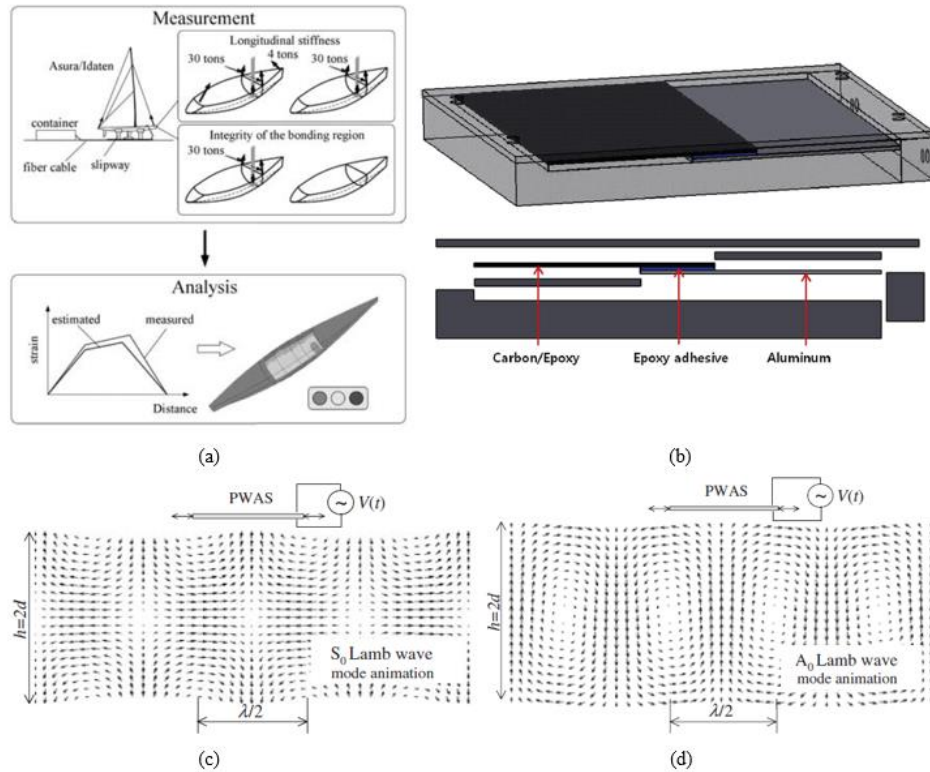
Figure 8. Failure detection of the joints; (a) Fiber-optic sensing by BOTDR [47], (b) Schematic diagram of the adhesion fixture of CNTs mixed epoxy [20] and PWAS interaction with lamb modes from [48]; (c) Symmetric lamb mode and (d) Antisymmetric lamb mode.

3. Part 1 – Multi-Material Joining between CFRPs and Metals

3.1. Part Introduction

The need for CFRP is growing, but it still has obvious limitations. For example, producing automobiles consisting entirely of CFRPs is realistically not possible not only because of material costs but also safety verification. This has naturally led to application of multi-materials parts into construction of hybrid structures, and therefore, joining of CFRP and metal has recently been studied extensively [1-20]. Mechanical fastening is intuitive and saves time, but it causes breakage of the composite and necessitates predrilled holes, resulting in stress concentration. Adhesive bonding does not require any holes and the load is distributed over a wide area, but the surface treatment of the material to be bonded is important and additional time is required for curing. Therefore, we tried to bond CFRP with metal through co-curing of the resin used as the matrix in the CFRP. Steel and aluminum, which are the most representative structural materials, were used as the metals for multi-material joining. The single-lap shear test was used to compare the adhesive strengths of single-lap joints bonded with co-curing and conductive epoxy to confirm that they have usable adhesive strength. Also, we confirmed the optimal point for increasing the adhesive strength of co-curing by surface treatment of metal.

3.2. Experimental

3.2.1. Materials

In this experiment, we used CFRPs fabricated with plain-woven carbon fiber (T300-grade provided by JMC Co., Korea) and unsaturated polyester (LSP-8020B from CCP Composite Korea Co., Korea) and stainless steel (SUS 304L) or aluminum (A1050) plates to manufacture the multi-material joining. For bonding of the single-lap joints, metal and CFRP were bonded using conductive adhesive (CW 2400 from Circuit Works) and unsaturated polyester.

3.2.2. Sample Preparation

First, the single-lap joints were manufactured according to ASTM D5868 specifications, as shown in Fig. 9. We fabricated five different types of samples based on various materials and joining conditions: CFRP-steel and steel-steel (conductive adhesive), CFRP-steel, CFRP- Al and CFRP-CFRP (co-curing). First of all, CFRP should be made with vacuum assisted resin transfer molding (VARTM). At first, steel and aluminum plates were rinsed with methanol and DI water. Carbon fiber textiles were cut into the desired size, and 9 plies were laminated on the metal surface. The stacked fibers were evacuated inside a vacuum bag using a vacuum pump, so fibers and metal were closed. After that, unsaturated polyester was used as the resin. 1 wt.% hardener was added to

13

the resin, stirred for 10 minutes, and impregnated into the carbon fiber. Then, the CFRP having the dimensions of 101.6 mm x 25.4 mm was demolding after being cured over-night. The CFRP surface was polished by a sand-paper and joined with steel by CW2400 which was mixed at 1:1 ratio. The adhesive was evenly applied to the surface, and the adhered area was clipped to allow a constant pressure to be applied to all of the samples to ensure stable curing.
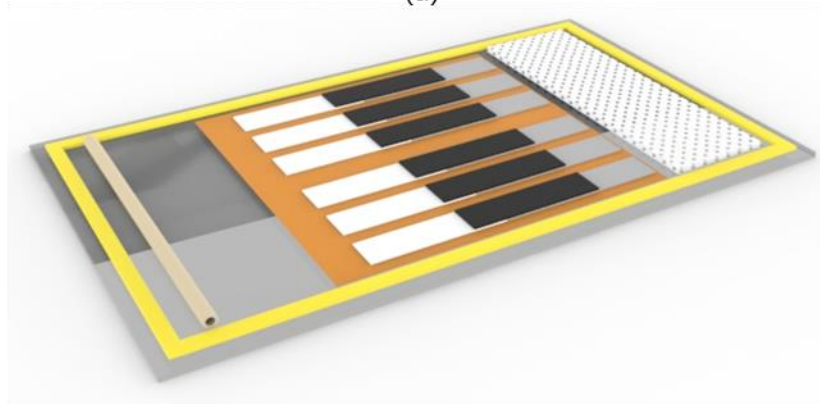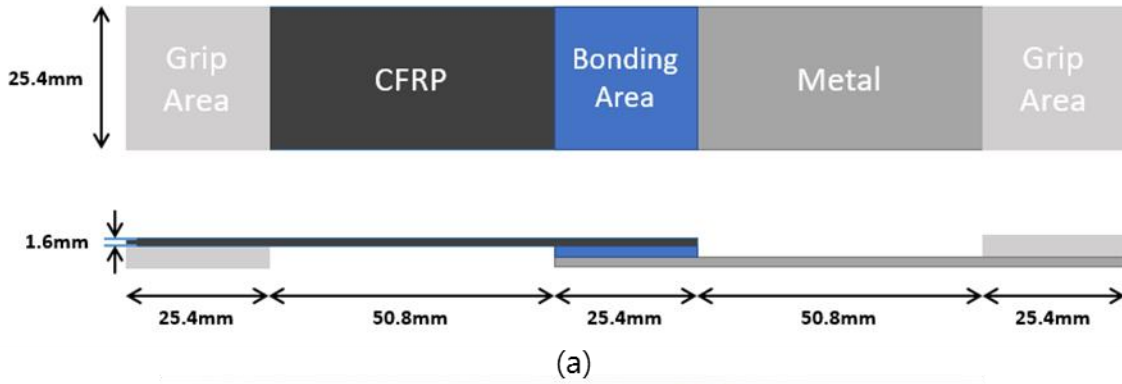
Figure 9. Schematic diagram of (a) dimension and (b) manufacturing of VARTM of the co-cured single-lap joints.

Next, co-cured joints were fabricated as follows – similar to the production method using a conductive adhesive, but the process is much simple: First, taping was performed to prevent contamination due to polyester except for the part to be bonded on the metal surface. The carbon fiber was cut to a desired size and then laminated on a metal or carbon fiber. 1 wt.% hardener was mixed in the polyester resin for 10 minutes, and the mixture was infused into the fiber using vacuum formed in the vacuum bag. Next day, demolding completes the simultaneous cured single-lap joints. This method is advantageous because it can simultaneously cure and join CFRP with VARTM alone. Co-curing method was used to join various combinations of identical and dissimilar materials, including steel with CFRP, aluminum with CFRP, and CFRP with CFRP.

14

To make bushing-inserted CFRPs rather than single-lap joints, a different process was needed. The size of the sample was changed because we had to perform push-out tests on the bushings instead of single-lap shear tests. Carbon fiber was cut to 50 mm x 50 mm, and 9 sheets were laminated like a single-lap joint. Then, a hole having a size of 8 mm was formed at the center of the carbon fiber using a circular punch. After inserting the inserts into the holes, samples were manufactured using VARTM. After a vacuum bag was placed, it was used as a vacuum process, and the polyester was used as a resin in the same manner as in the other cases, and a 1% hardener was stirred for 10 minutes and then impregnated. Manufactured samples had a size as shown in Fig. 10. The important thing in manufacturing this sample is to prevent the resin from sticking around the bushing.
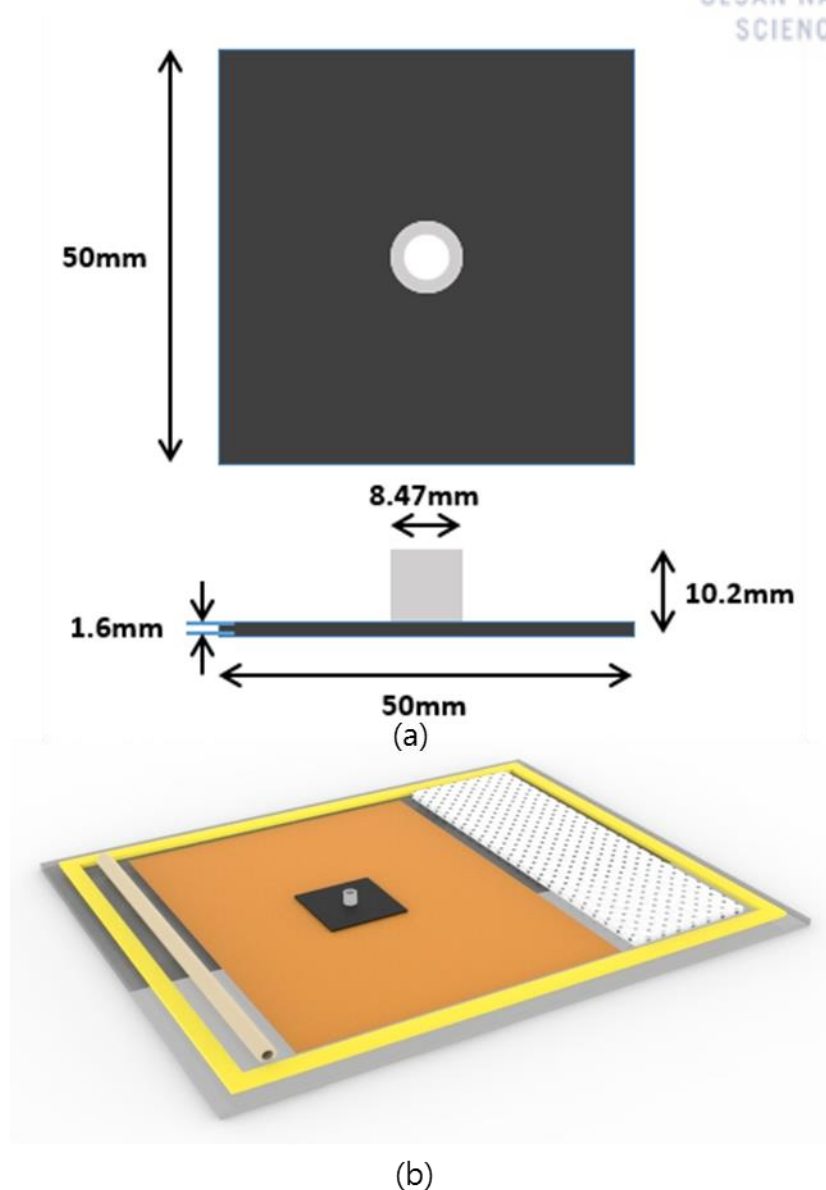
Figure 10. Schematic diagram of (a) dimension and (b) manufacturing of the bushing-inserted CFRPs.

Here, the metal used in the sample preparation was sized to 101.6 mm x 25.4 mm using wire cutting. The metal surface was cleaned with MeOH to remove oil and carbon contaminants.

Next, the metal surface was subjected to plasma treatment. Atmospheric plasma treatment was adopted and compressed dry air was used as the gas. The distance between the sample and the plasma nozzle was adjusted to 5 mm, and the nozzle speed was shifted to 2 m/min. This steel and aluminum surface were treated with plasma 10, 20, 30, 40 and 50 times and then joined using VARTM. Steel bushing was also plasma-treated. Since the bushing is cylindrical, one side is plasma-treated and then the other side is plasma-treated.

16

3.2.3.   Characterization

To characterize the manufactured samples, a single-lap joint was subjected to a single-lap shear test and bushing-inserted CFRPs were subjected to a push-out test. A universal test machine (UTM), Instron 5982, was used for this test. A single-lap shear test was used for the tensile test jig, and a push-out test was used for the compression test jig. The single-lap shear test was carried out at an extension rate of 1.3 mm/min according to the ASTM D5868. The push-out test had a compressive extension rate of 1.3 mm/min as shown in Fig. 11.
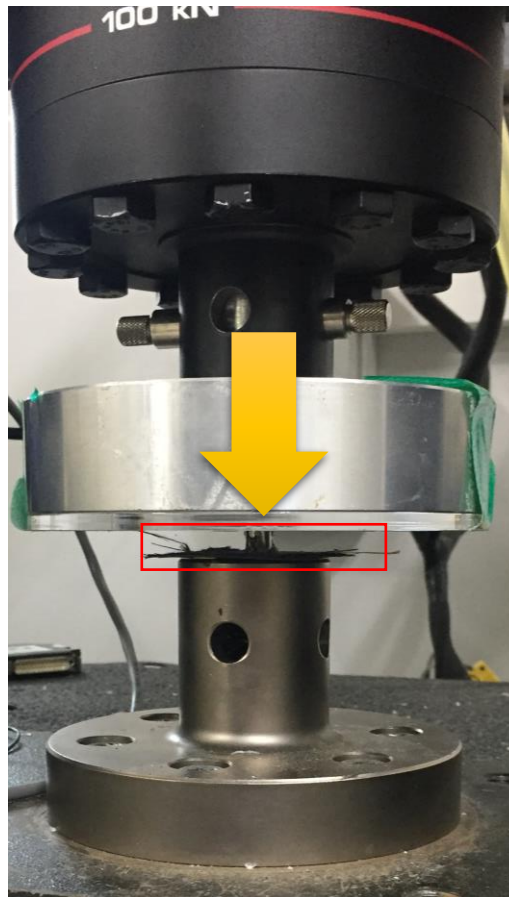
Figure 11. Experimental setup picture of push-out test.

In order to improve the adhesive strength of the co-cured joints, the metal surface was subjected to atmospheric pressure plasma treatment. The plasma treatment was performed according to the conditions in Table 1, and Fig. 12 shows the schematic of plasma treatment. It was considered to be one plasma stroke when the plasma nozzle passed the metal surface once.

Table 1. Atmospheric plasma treatment conditions.

Speed	**2m/min**
Nozzle height	**5mm**
Gas type	**Compressed dry air**
Power	**850W/50Hz**
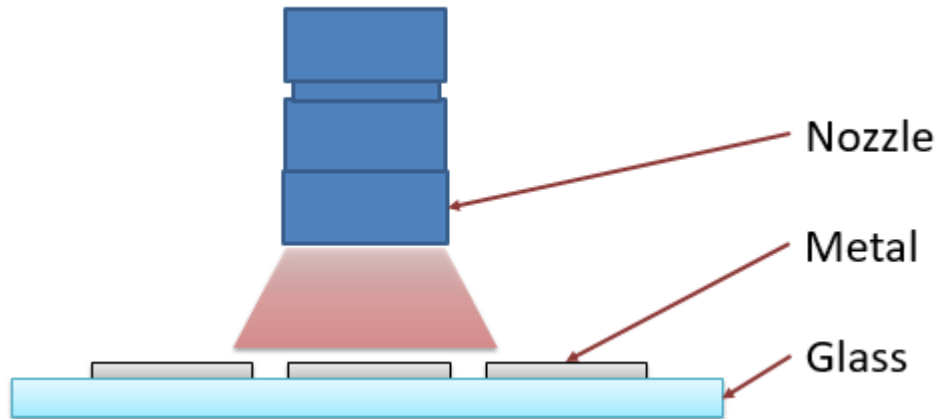
Figure 12. Schematic diagram of the plasma treatment for the metal surfaces.

As the roughness of the surface increases, the adhesive strength becomes higher due to mechanical interlocking. Therefore, we used a 3-dimensional surface measurement system (Model NV-3000 from Nanosystem) to identify roughness and 3-dimensional topology changes of the metal surface after plasma treatment. By using this equipment, it is easy to compare roughness because the RMS surface roughness value of the surface can be quantified. In addition, due to the chemical composition change of the metal surface, the bonding strength with the resin becomes strong and the adhesive strength increases. Therefore, contact angle measurement (Model Phoenix 300 from SEO) and X-ray Photoelectron Spectroscopy (XPS, Model K-alpha from ThermoFisher) were carried out in order to investigate the chemical effects.

3.3. Results and Discussion

3.3.1. Adhesive Strength of Single-Lap Joints

A single-lap shear test was performed using an Instron to obtain the adhesive strength. Five single-lap joints (Co-cured CFRP-Aluminum, CFRP-steel, CFRP-CFRP single-lap joints and CFRP-steel and steel-steel single-lap joints joined by conductive adhesive) were tested. The results of the experiment are shown in Fig. 13. Comparing the experimental results, the adhesive strength and the fracture strain are significantly different depending on which materials and the joining method used. CFRP-aluminum single-lap joints joined by co-curing have the weakest adhesive strength at 1500 N or less and the strain is low. CFRP-CFRP single-lap co-cured joints have the greatest strain.
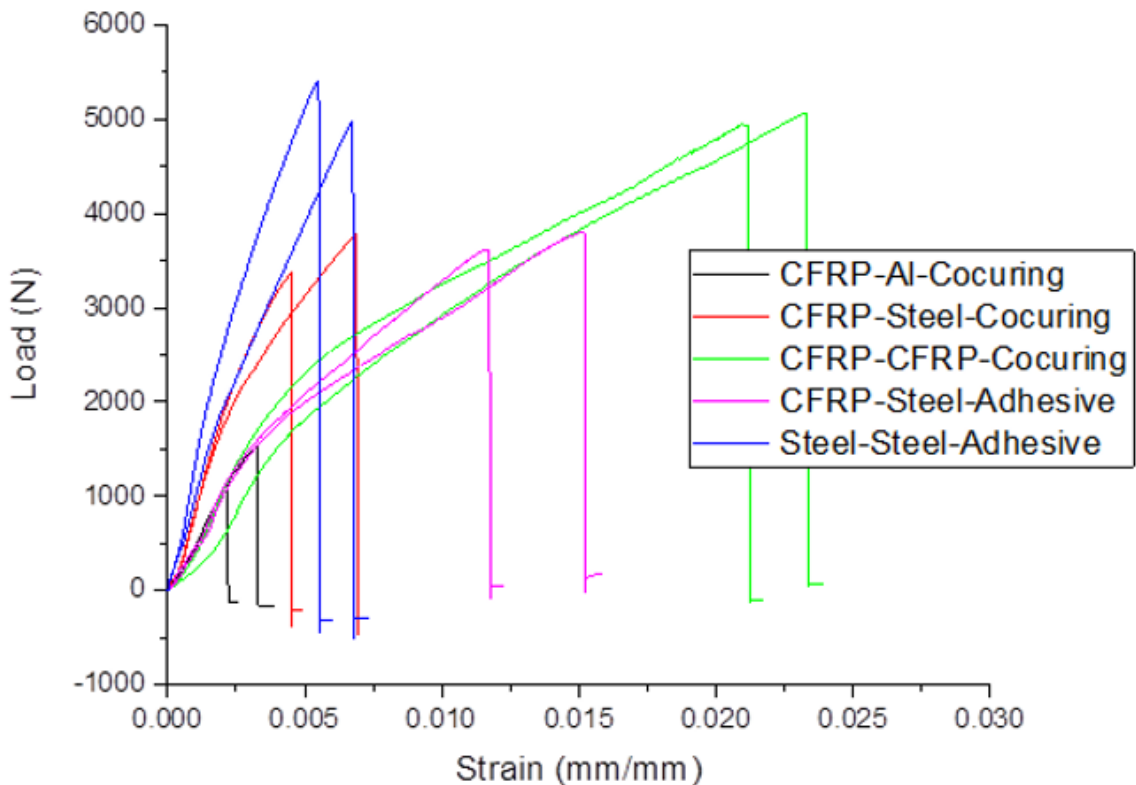
Figure 13. Force-strain curve of single-lap joints.

The graph of adhesive strength is shown in Fig. 14. The three joints on the left are joints joined by co-curing, and the joints on the right are joined with conductive adhesive. In general, the adhesive strength of the conductive adhesive is stronger than that of the co-curing. However, when the CFRP and steel joints with different joining methods, the adhesive strength between the co-curing and the conductive adhesive is not significantly different, but the adhesive strength of the conductive adhesive shows a stronger strength. As a result, there is no significant difference in

19

adhesive strength between the conductive adhesive and the co-curing, so the co-curing, which has a great advantage in productivity, is more advantageous for the multi-material joining.
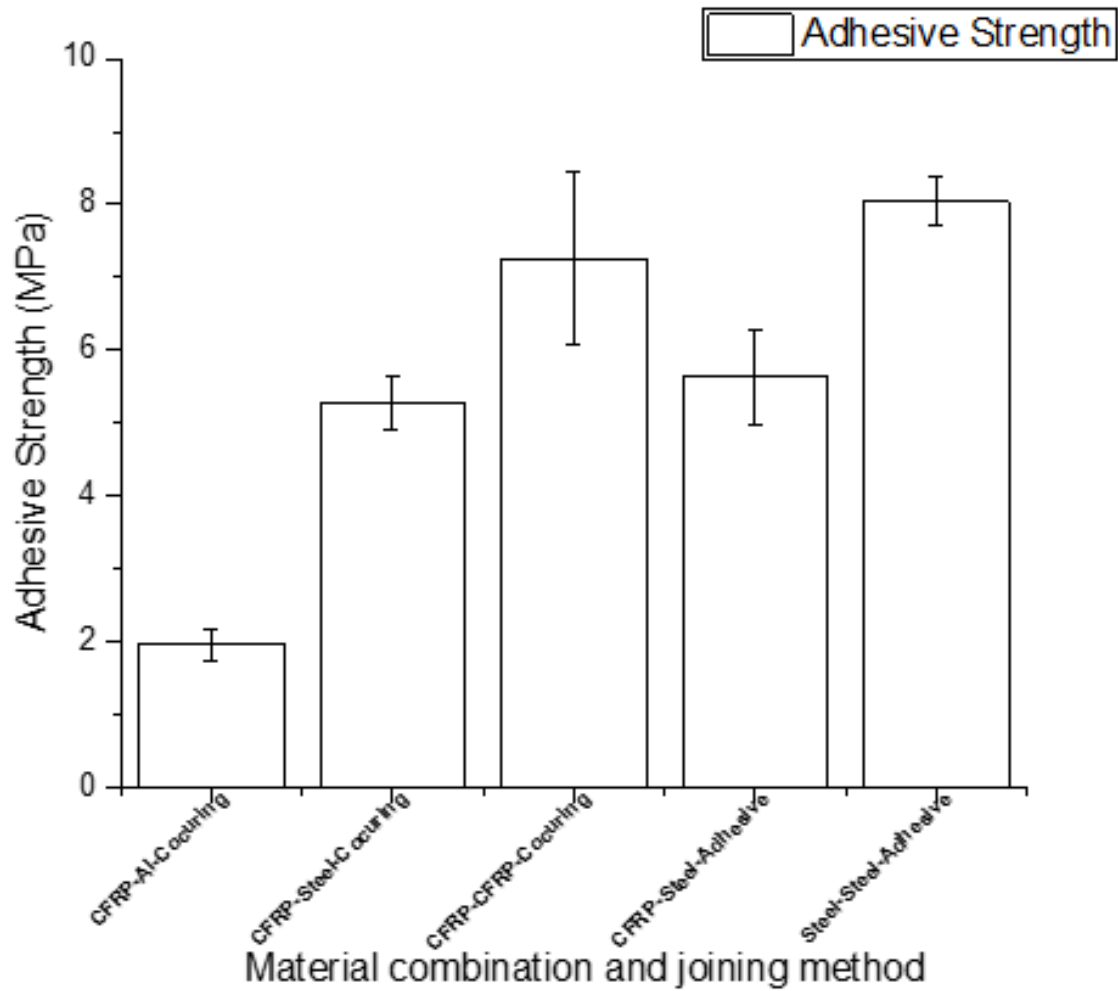
Figure 14. Average strength of each single-lap joints; Co-cured (CFRP-Al, CFRP-steel and CFRP-CFRP) joints and (CFRP-steel and steel-steel) joints joined by conductive adhesive.

3.3.2.   Shear Strength of Steel Bushings

  Push-out tests were carried out to measure the shear strength of bushing-inserted CFRP joined by co-curing. The samples were manufactured differently. The first sample had about 45 degrees of cured pure resin around the steel bushing and the second sample was made by removing the pure resin as shown in Fig. 15 (a) and (b). (a) of Fig. 16 is the push-out test result of the sample with pure resin and Fig. 16 (b) is the result of the sample without pure resin. Fig. 16 (c) shows the combined graph between Fig. 16 (a) and Fig. 16 (b). Resin rich sample shows about twice the shear strength of the resin poor sample. However, this result includes the adhesive strength of the pure resin and the CFRP as well as the adhesive strength of the bonded region by the co-curing of CFRP and metal. Therefore, when referring to the Fig. 16 below, it is important to make not to leave the resin except CFRP as much as more resins affect the push-out test, the sample have to be produced after the plasma treatment was made without pure resin.
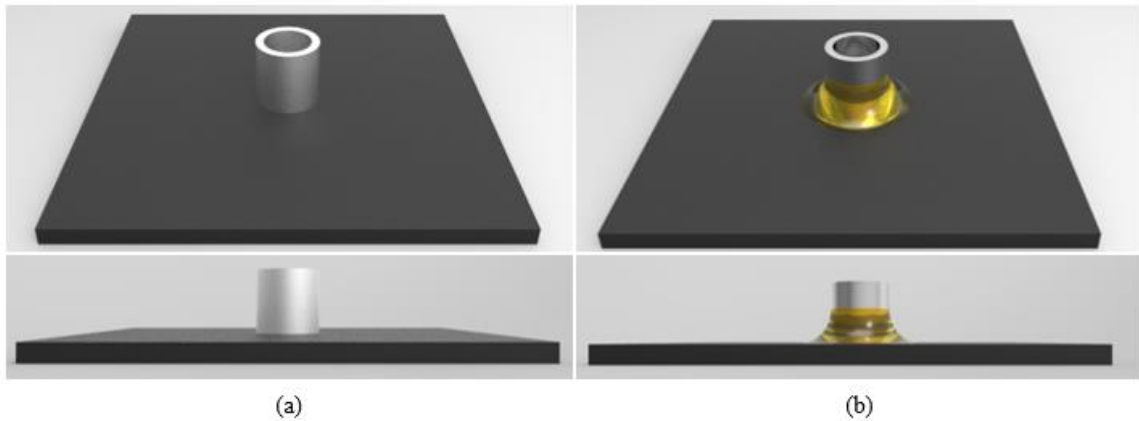
Figure 15. Schematic diagram of the (a) resin poor and (b) resin rich samples around the bushings.
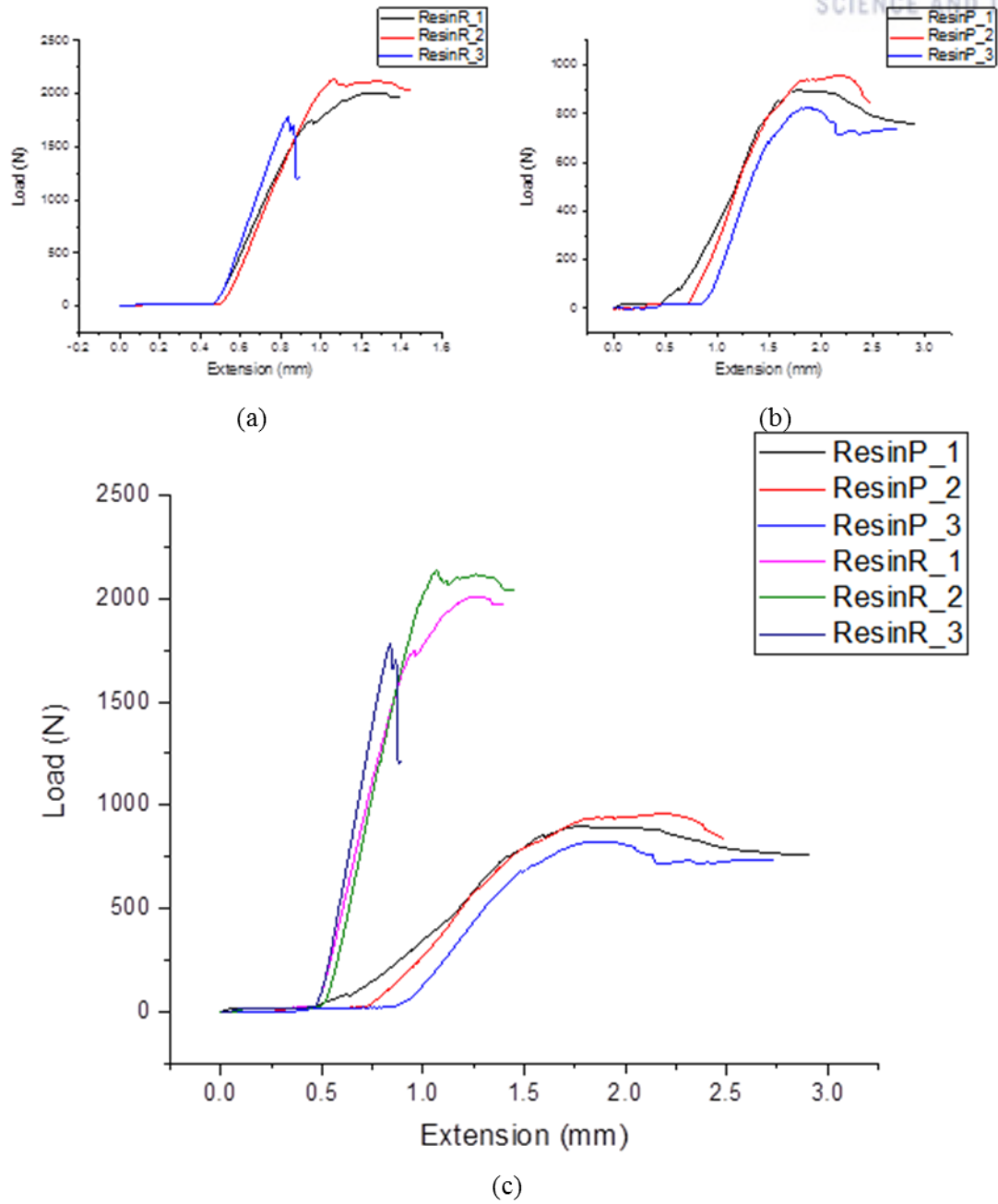
Figure 16. Force-displacement curve of (a) resin poor and (b) resin rich around the bushings, (c) combined graph of (a) and (b).

3.3.3. Atmospheric Plasma treatment

Generally, plasma treatment has several advantages and is frequently used in the process. First, carbonaceous contamination of the material surface will be removed, and functional groups like carboxylic acids are attached to the surface. These functional groups enhance the bond strength by forming strong chemical bonds with the materials for the coating or adhesive. In addition, polar hydroxyl groups make more hydrophilic surfaces, which help create intimate contacts between the adhesive and the metal surfaces as shown in Fig. 17. [50].
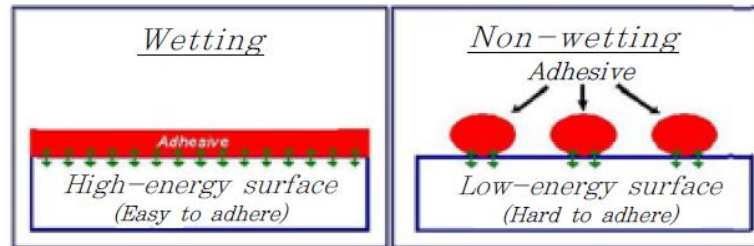
Figure 17. Schematic of the difference related with the wettability for the metal surfaces [50].

In the results of single-lap shear test, the adhesive strength of co-cured CFRP-aluminum single-lap joints were very low, so a solution was needed. Generally, in the case of bonding, the adhesive strength can be improved by surface treatment. As the surface treatment method, there are a method of increasing the surface roughness mechanically to improve the adhesive strength and a method of chemically treating the surface to increase the chemical bonding strength. In this experiment, metal was surface-treated with atmospheric plasma.

Fig. 18 (a) and (b) shows the adhesive strength change to multi-material joining of steel and aluminum with CFRP depending on the degree of surface treatment. It can be seen that the adhesive strength of both metals increases more than that of non-surface-treated metals. When the plasma treatment was performed 30 times (i.e., 30 strokes), the maximum adhesive strength was shown to be stabilized. Steel was increased to 6.6 MPa at the adhesive strength of about 5.2 MPa, and the adhesive strength was increased about 3 times at about 2 MPa to 6 MPa of CFRP-aluminum co-cured single-lap joints.
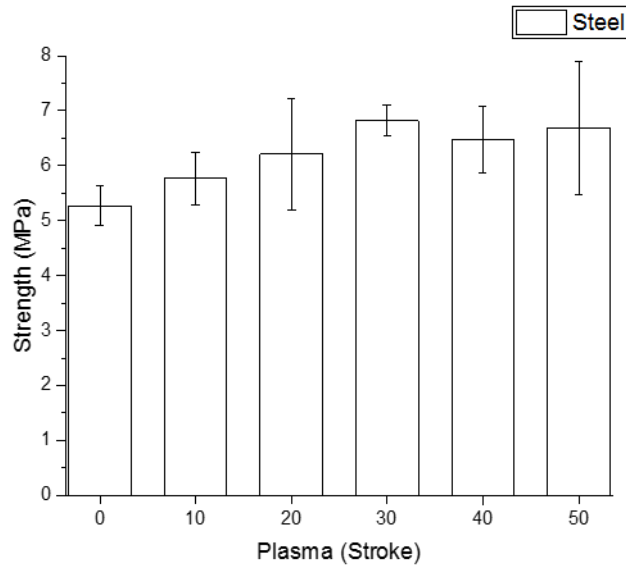
(a)
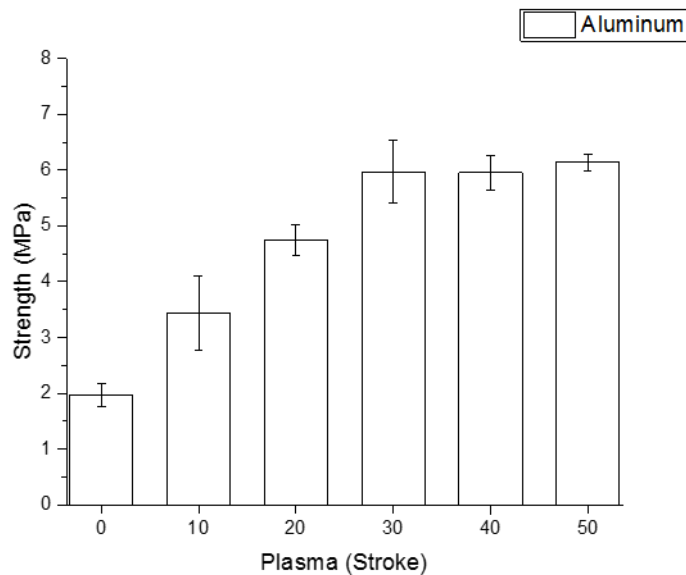
(b)

Figure 18. Adhesive strength of the plasma-treated single-lap joints; (a) CFRP-steel co-cured joints and (b) CFRP-aluminum co-cured single-lap joints.

Co-cured CFRP-aluminum single-lap joints showed a 3-fold increase in adhesive strength, so we investigated how much the adhesive strength increases when plasma performed 10, 20, and 30 strokes for bushing surfaces, respectively. Because the side of the bushing needs to be plasma-treated, the plasma treatment time is doubled compared to single-lap joints. Plasma processing conditions in previous experiments are very harsh conditions, so the plasma treatment of the

bushing was performed only 30 times under the condition that the distance between the sample surface and the nozzle was 5 mm and the nozzle speed was very slow, 2 m/min.

As a result of the push-out test, Fig. 19. The results show that the adhesive strength between steel bushing and CFRP is considerably stronger than that of single-lap joints. In addition, as the number of strokes of plasma treatment increases, the adhesive strength tends to gradually increase. However, the contact area between CFRP and bushing is very small compared to single-lap joints, so the plasma treatment effect does not appear to be significant.
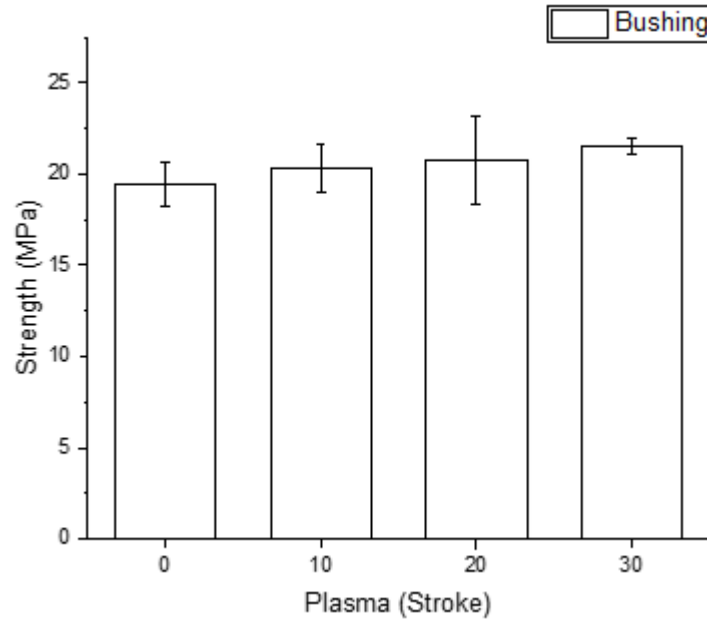
Figure 19. Adhesive strength of the plasma-treated bushings.

3.3.4. Surface Analysis

Two measurement experiments were performed to analyze the cause of the increase of adhesive strength after plasma treatment. First, the surface roughness before and after the plasma treatment was measured by 3-dimensional surface measurement. The RMS values before plasma treatment were an average 1.346 µm for steel and 449.7 nm for aluminum.

Although it was difficult to measure the exact RMS change after plasma treatment at the limit of resolution (0.5 µm). According to Tang [51], the SUS 304l was subjected to atmospheric plasma treatment (Model ATMOS, Plasmart Korea) using argon gas for 60 seconds at 120W, the RMS value is rather reduced. Next, as shown in Fig. 20, the topology of the metal surface before and after the plasma treatment was not significantly different. The increase in adhesive strength due to mechanical factors does not seem to have a significant effect through the paper and Fig. 20.

25
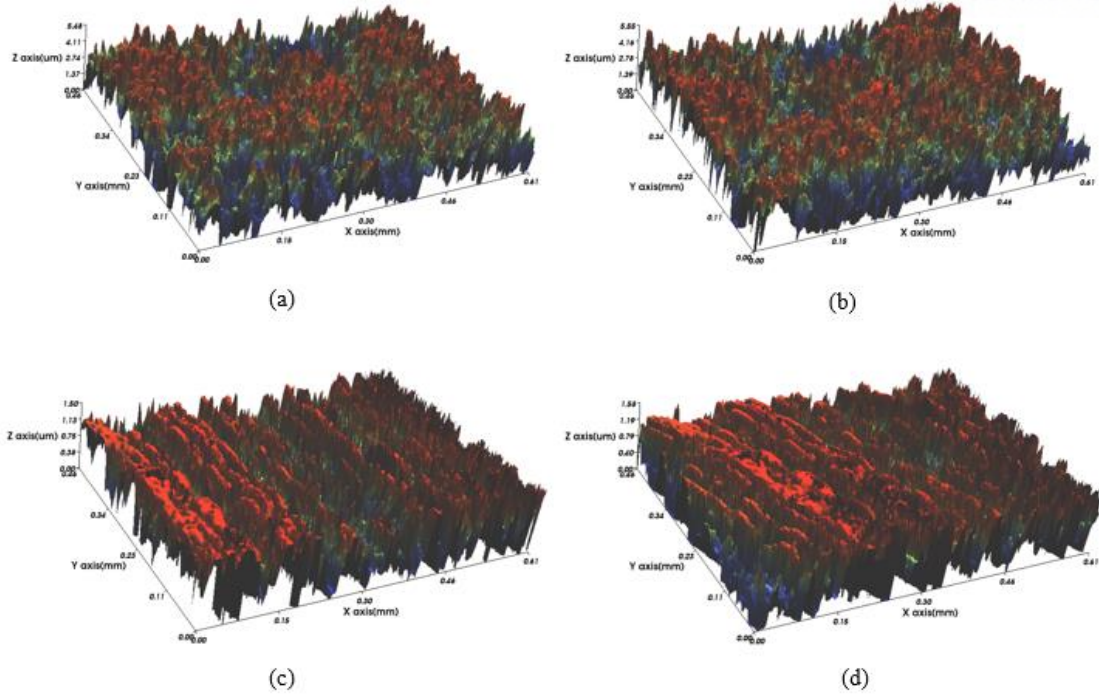
Figure 20. Surface topology of the steel and aluminum before and after plasma treatment; (a) Non-plasma-treated steel with 1.15 **μm** RMS value, (b) Plasma-treated steel with 1.12 **μm** RMS value, (c) Non-plasma-treated aluminum with 397.98 nm RMS value and (d) Plasma-treated aluminum with 414.47 nm RMS value.

Contact angle measurement and XPS analysis were performed to analyze the cause of the adhesive strength change by chemical factors. Fig. 21 shows that the contact angles of both steel and aluminum decrease after 10 strokes plasma treatment. Figure 22 shows the change of the contact angle according to the degree of plasma treatment, and the contact angle decrease rate of aluminum is larger than that of steel. The contact angle of the both metals is the smallest when 30 strokes plasma treatments are performed, and the contact angle is slightly increased thereafter.
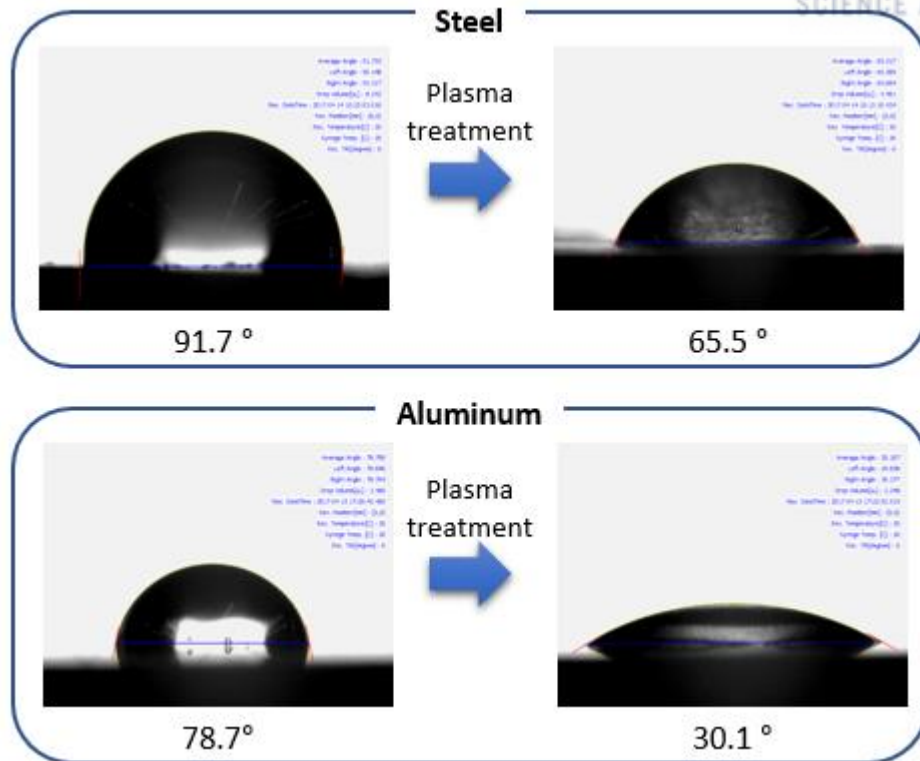
Figure 21. Reducing the contact angle after plasma treatment for both metal surfaces.
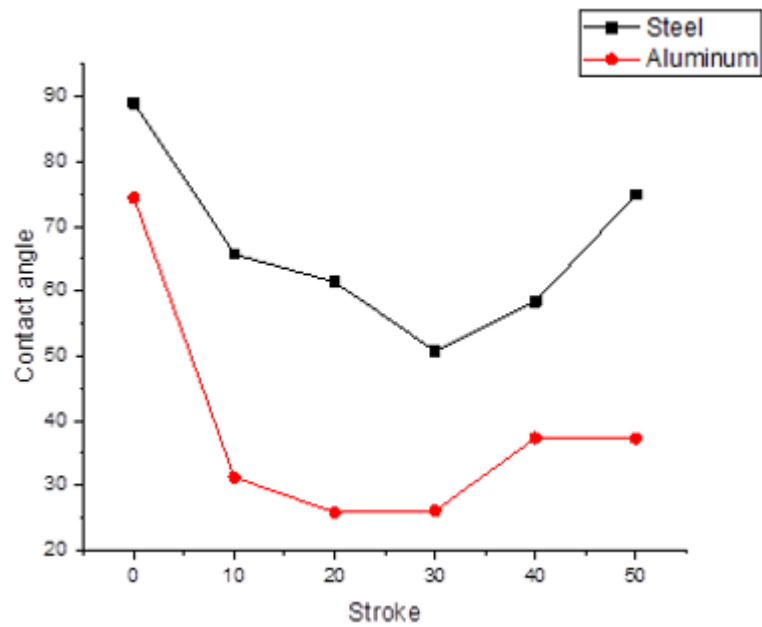
Figure 22. Contact angle-plasma strokes curve for both metals.

This is compared with the XPS results as follows. Fig. 23 (a) shows a C1s spectra of 10 strokes plasma-treated steel. The surfaces of steel have three peaks. In this graph, the peak 1 at 284.5 eV is

C - C bonding and the peak 2 at 286.4 eV is C - O bonding. The peak 3 at 288.5 eV is related with C = O bonding. Fig. 23 (b) shows the C1 spectra of 10 strokes plasma-treated aluminum plates. The C1s spectra from the non-treated metal surface to 50 strokes to the plasma-treated metal surface were obtained and the component % of C - C, C - O and C = O are shown in the following Tables 2 and 3. This tables show that the ratio of C = O was the highest when 30 times of plasma treatment was applied to both steel and aluminum. As the carboxylic acid functional group increases, the adhesive strength was increased due to the increasing of hydrogen bonding.
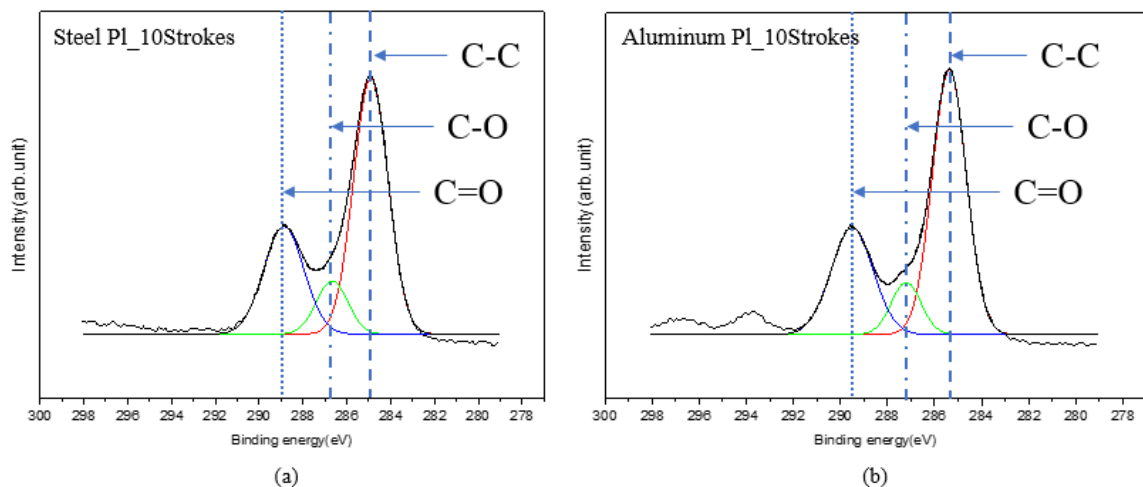
Figure 23. C1s XPS spectra of (a) 10 strokes plasma-treated steel and (b) 10 strokes plasma-treated aluminum.

Table 2. The component ratios of the steel surface from the results of the C1s XPS spectra.

Component ratio %	C-C	C-O	C=O
Untreated steel	33.2	32.7	34.1
10 Strokes	32.6	29.6	37.8
20 Strokes	37.4	23.7	38.9
30 Strokes	33.6	25.2	41.2
40 Strokes	32.5	29.6	37.9
50 Strokes	21.4	50.2	28.4

Table 3. The component ratios of the aluminum surface from the results of the C1s XPS spectra.

Component ratio	C-C	C-O	C=O
%			
Untreated aluminum	29.3	35.1	35.6
10 Strokes	32.2	28.1	39.7
20 Strokes	30.3	30.4	39.3
30 Strokes	24.4	24	43.6
40 Strokes	30.6	32.1	37.3
50 Strokes	29.2	42.1	28.7

Comparing the contact angle and the component ratio through the C1s spectra of XPS after plasma treatment, the surface of 30 strokes plasma-treated metal showed the highest hydrophilicity and the highest carboxylic acid functional group ratio. As a result, the plasma treatment increases the hydrophilicity of the metal surface, which leads to an intimate contact between the adhesive and the metal surface, thereby increasing the adhesive strength. And the carboxylic acid group on the metal surface was increased, so that the number of hydrogen bonding was increased, which increases the adhesive strength. However, when the plasma treatment exceeds 30 strokes, the contact angle is increased and the C = O components are decreased, so that the adhesive strength is not increased any more. The reason of this phenomenon is that ions may transfer to non-active particles due to long-term exposure of plasma [52, 53] and non-active particles have negative effects on contact angle and adhesive strength [51].

3.4. Summary

To measure the adhesive strength of multi-material joining, we fabricated single-lap joints and bushing-inserted CFRP joined by co-curing. A single-lap joint was also fabricated with conductive adhesive bonded to the control sample. In order to join the CFRP to the metal by co-curing, unsaturated polyester of CFRP was used and these samples were all manufactured via the VARTM process. The multi-material joining showed lower adhesive strength than the same-material joining. Generally, single-lap joints bonded with conductive adhesive have stronger adhesive strength than co-cured joints. As a result, it was found that the co-cured multi-material joints show the lowest adhesive strength. However, the adhesive strength of the co-cured multi-material joints was improved by plasma treatment. Plasma treatment increases the hydrophilicity of the metal surface and facilitates the contact between the polyester resin and the metal surface, which helps to improve the adhesive strength. In addition, the number of polyether and hydrogen bonds increases with the increase of the carboxylic acid functional groups, and the adhesive strength increases.

Through this experiment, it was confirmed that the adhesive strength of the multi-material joining by the co-curing is good. Particularly, it was found that the adhesive strength between aluminum and CFRP co-cured single-lap joints after plasma treatment was improved by about 300%, and the adhesive strength of steel was also improved. Co-curing of the most commonly used aluminum and steel provides stable joint strength, which will contribute to the expansion of CFRP parts in the future.

4. Part 2 – Structural Health Monitoring of CFRP-Metal Junction

4.1. Part Introduction

In this section, a study on SHM of co-cured single-lap joints through electrical resistance measurement is presented. We investigated the initiation, propagation of cracks and de-bonding at the joints by measuring the electrical resistance change. CFRP-steel joints and steel-steel joints joined by conductive adhesive, and CFRP-steel, CFRP-aluminum and CFRP-CFRP co-cured joints were tested by measuring the electrical resistance in real time during a single-lap shear test. In addition, we confirmed through experiments that CFRP and steel bushing joined by co-curing can also detect the failure by measuring the electrical resistance change.

The Kelvin resistance measurement was used to measure the resistance in real-time. The Kelvin resistance measurement can reduce the contact resistance significantly compared to the 2-probe resistance measurement by measuring the electrical resistance using four probes.

As a result, failures in CFRP-metal multi-material joints produced by co-curing could be detected by monitoring electrical resistance.

4.2. Experimental

4.2.1. Materials

In this research, plain-woven carbon fiber (T300 grade provided by JMC Co., Korea) was used for the reinforcement of CFRP and unsaturated polyester (LSP-8020B from CCP Composite Korea Co., Korea) and hardener (Lupeox methyl ethyl ketone peroxides from ARKEMA Co.) were used for the polymer matrix. Also, conductive epoxy (CW 2400 from Circuit Works) was used to form multi-material joints. It consists of adhesive and hardener, mixed at 1:1 ratio and spread over the adherend. In order to measure the resistance between different materials, an electrical wire was connected to the material surfaces with silver paste (Elcoat P-100 from CANS).

4.2.2. Sample Preparation

Samples for the SHM of joint failure using electrical resistance were prepared in two types. The first is a standard for single-lap joints in accordance to ASTM D5868. The second was a bushing-inserted CFRPs for push-out tests.

Basically, how to manufacture a sample is described in Section 3.2.2. However, more complex processes are required in this part because the electrical resistance must be measured. In the preparation of VARTM, the wire was inserted on the top layer of carbon fiber and the electrode was fixed by silver paste, then vacuum was applied and carbon fiber was impregnated by polyester.

After curing, the sample was demolded, the tape on the metal surface was removed, and the electric wire and the metal surface were connected using silver paste.

The fabricated samples are 5 different types; CFRP-steel and steel-steel joined by conductive adhesive and CFRP-steel, CFRP-aluminum and CFRP-CFRP co-cured single-lap joints.

4.2.3. Characterization

Electrical resistance was measured using Keithley digital multimeter (DMM) 2002 for SHM of the junction as shown in Fig. 24. 2-probe and 4-probe methods were used to track the change in electrical resistance due to deformation of the joint during single-lap shear test. 2-probe is the simplest way to measure electrical resistance, where the voltage is measured by flowing a constant current between two electrodes. Therefore, although the measuring method is simple, the resistance to be measured may have an error due to the contact resistance. On the other hand, 4-probe measure resistance using four electrodes. The current is applied to the sample at both end electrodes, and the voltage is measured between the two inner electrodes, and the resistance is calculated by the Ohm's law. Therefore, the effect of contact resistance is smaller than that of 2-probe, which is advantageous for more precise resistance measurement. The wire connected to the sample was connected to a multimeter to measure the internal resistance change.
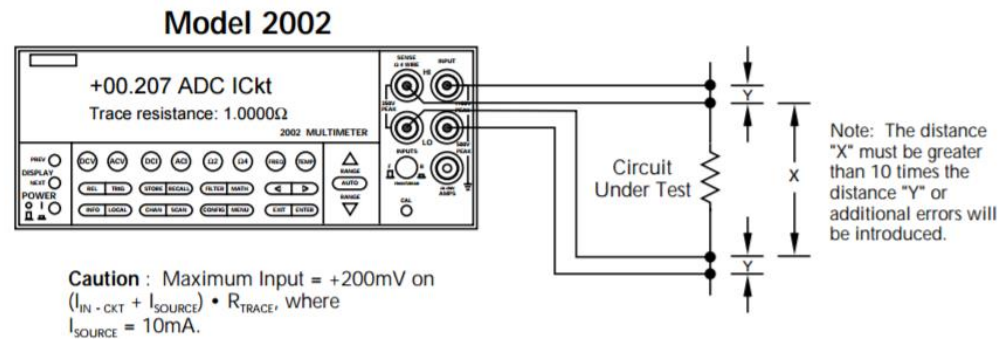
Figure 24. Schematic of the 4-probe resistance measurement by DMM 2002.

The load was applied to the sample using the Instron UTM. Single-lap joints were tested using a jig for tensile and bushing-inserted CFRPs were measured for load and strain applied to a sample using a compression jig. Using the measured load, strain and resistance changes, it was confirmed that SHM was feasible by electrical resistance.

In order to analyze the cause of the electrical resistance change during the test, the fractured surfaces were measured by an optical microscope (Model NV150N from Nikon). The surface of

the fractured co-cured joints and the surfaces of the joined by conductive adhesive joints were analyzed. Each surface was observed by magnifying 5 times.

4.3. Results and Discussion

4.3.1. Pre-Test and Single-Lap Joint Using 2-Probe Resistance Measurement

First, a peel test was carried out to check the failure detection of the joint using electrical resistance. As shown in Fig. 25, the following peel test was used for the 3-point bending test to see if the increase of the electrical resistance due to the reduction of the contact area of the joint because the breakage of the joint occurred slowly compared to the single-lap shear test. The heading speed of the jig is 1 mm/min and has 70 mm support span. Experiments were carried out using CFRP-steel co-cured joints. In Fig. 26 as the load increases, the electrical resistance increases at the beginning of the crack, and the electrical resistance gradually increases as the crack progresses. Based on this, it is confirmed that the contact area of the joint and the electric resistance between the two materials are related.
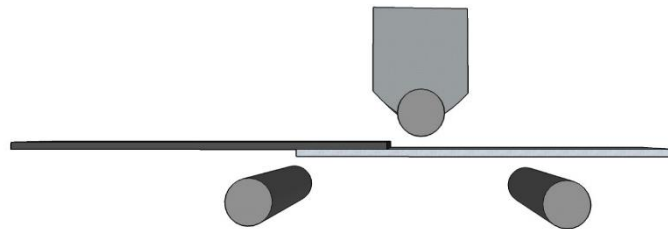

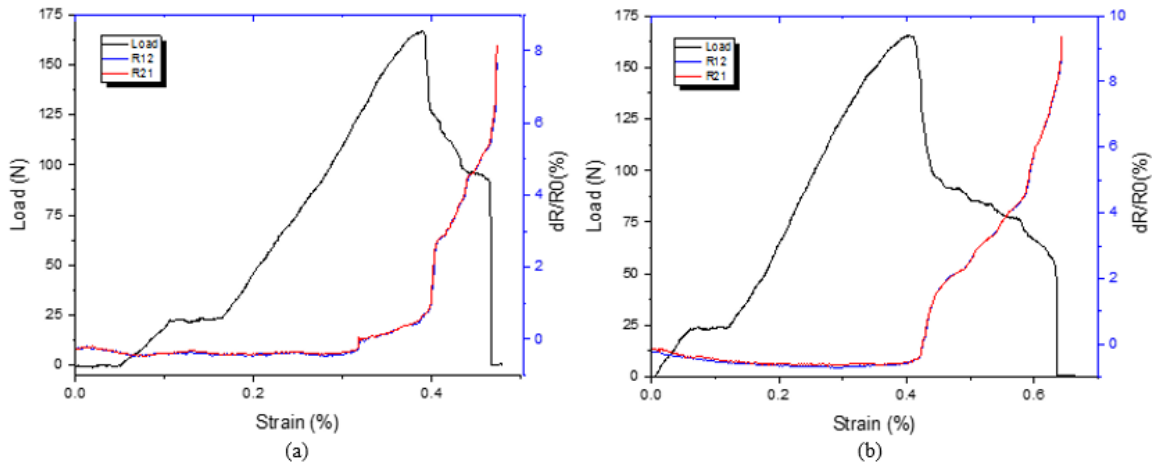**Figure 25.** Schematic diagram of the 3-point bending for the pre-test.

Figure 26. Force-resistance change rate during the 3-point bending test.

Therefore, we tested co-cured CFRP-steel single-lap joints. Electrical resistance was measured using 2-probe measurement. The load change and the electrical resistance change of the single-lap shear test are shown in Fig. 27 (a) and (b). Comparing the results, when the load is applied to the sample, the electrical resistance decreases and the resistance begins to increase during the test. The tendency of the electrical resistance to increase significantly was observed in all samples when complete failure of the joint occurred, but the electrical resistance change during the experiment did not have a uniform tendency. The reason for this is that in case of 2-porbe measurement, it is difficult to measure the electrical resistance change due to the single-lap-shear-induced change in the joint because the contact resistance at the electrode greatly acts and the initial resistance value is high. Therefore, if the rate of change in resistance due to the contact area change is within 1%, it is greatly affected by the resolution of the measuring multimeter. For the Keithley DMM 2002 model, the measurement error is less than 1%. Thus, Fig. 27 (a), the resistance increases during the test due to measurement error. In order to solve this problem, the experiment was carried out using 4-probe measurement which is less influenced by contact resistance.
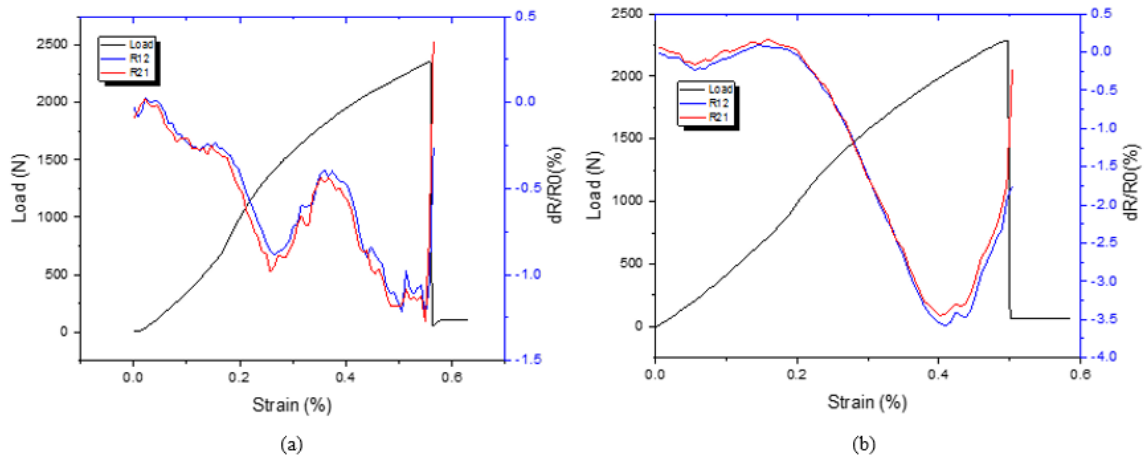

Figure 27. Force and resistance change rate during single-lap shear test.

4.3.2.　SHM of Single-Lap Joints Joined by Conductive Adhesive

First, SHM of single-lap joints joined with conductive adhesive was performed. Fig. 29 shows the experimental result of single-lap joints of CFRP-steel joined with conductive adhesive. In the graph, the electrical resistance tends to decrease gradually as tension increases. However, it is difficult to confirm the increase of the resistance due to the occurrence of cracks or the reduction of the contact area. Fig. 29 (b) shows a slight increase in electrical resistance before failure. This is due to the detaching of the carbon fiber layer, not the crack at the joint. Fig. 39 (a) and (b) are a photograph of broken CFRP-steel single-lap joints joined by conductive adhesive. Cohesive failure occurs in Fig. 39 (b). As shown in Fig. 29 (a), when cracks cannot be detected due to electrical resistance but it can be detected that the occurrence of fiber tear failure by slightly increased electrical resistance before fracture as shown in Fig. 29 (b). In this case, the CFRP surface was not uniformly polished during the grinding process, so that the broken carbon fibers adhered to the conductive adhesive and detached. Therefore, electrical resistance was increased a little before the joint failure due to the CFRP breakage.

Figure 28. Schematic diagram of the CFRP-steel single-lap joints joined by conductive adhesive.

Figure 29. Force-resistance change rate of the CFRP-steel joints during the test, resistance measured by 4-probe method.

The experimental results from steel-steel single-lap joints joined with a conductive adhesive are shown in Fig. 31. The decrease in electrical resistance of steel-steel single-lap joints is related to the deformation of the joint. As shown in Fig. 32, The distance of the junction decreases during the

35

experiment, then the electrical resistance decreases. The reason of the increase in resistance before the failure is the decrease of contact area due to the crack developed in the adhesive. However, the resistance change in the conductive adhesive is too small to be measured in the SHM of the CFRP-steel single-lap joints. Therefore, in Fig. 29, The resistance is greatly increased only when the materials are completely de-bonded without any change in electric resistance due to cracking before fracture, so that the crack cannot be detected at the joints. As a result, it was difficult to detect cracks using electrical resistance in joints bonded with a conductive adhesive.
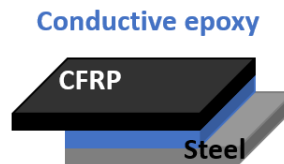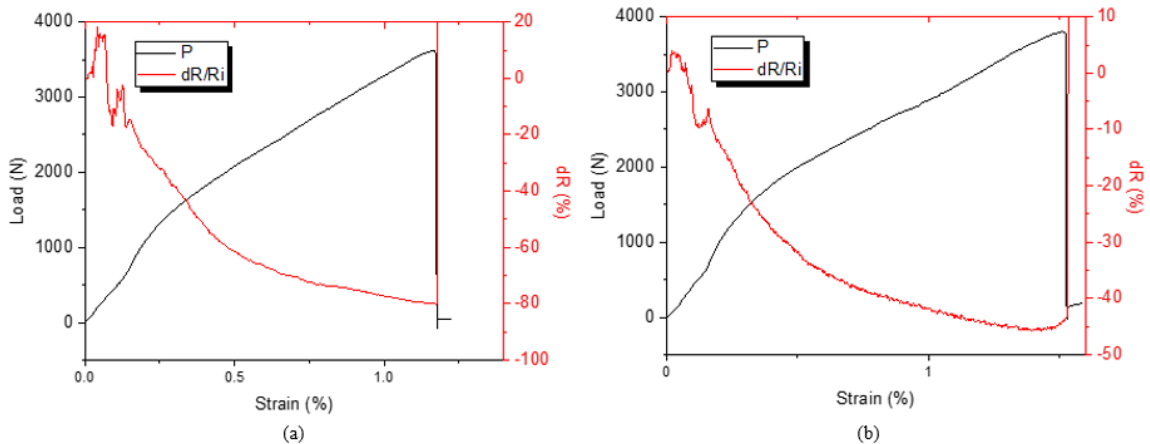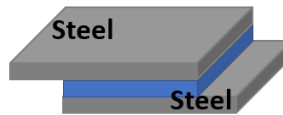

Figure 30. Schematic diagram of the steel-steel single-lap joints joined by conductive adhesive.
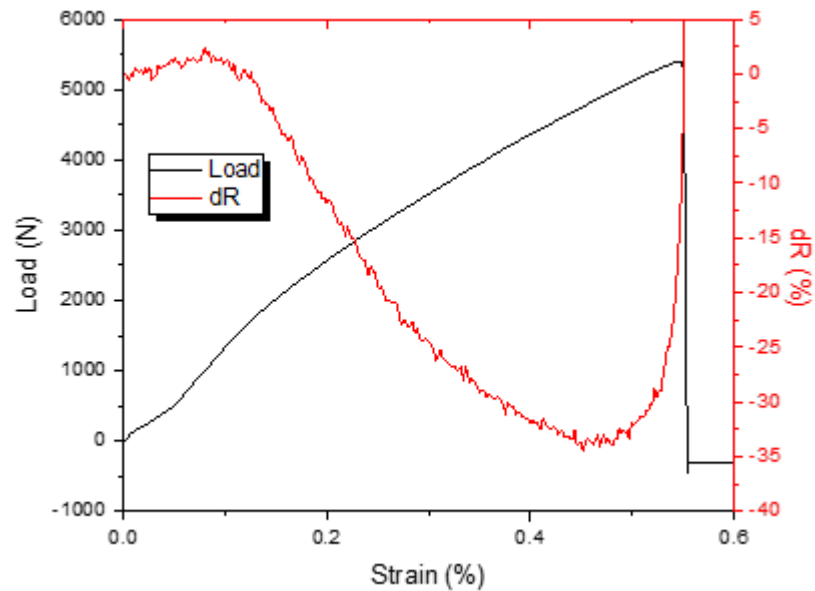
Figure 31. Force and resistance change rate of the steel-steel joints during the test, resistance measured by 4-probe method.

Steel

Conductive
adhesive

Steel

$$R = \rho \frac{l}{A}$$

$A = const, but\ l\ will\ be\ decreased$
It makes resistance decrease
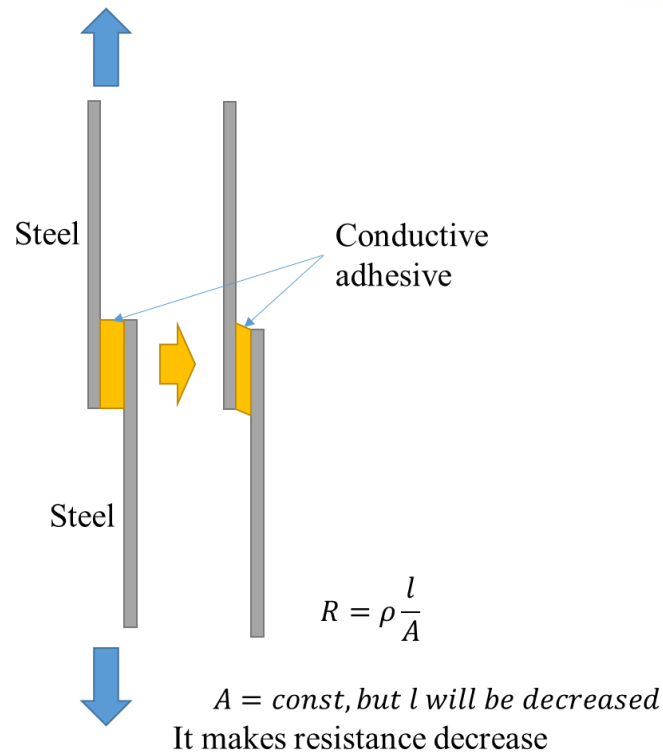
Figure 32. Schematic of the change of the adhesive region during the test.

4.3.3. SHM of Co-Cured Single-Lap Joints

For CFRP-steel co-cured single-lap joints, Fig. 34 shows the test results. Co-cured joints showed a significant change in electrical resistance due to the reduction of the contact area of the joined surfaces, since the carbon fibers and the metal directly contact each other. Therefore, as shown in Fig. 34 (a) and (b), the point at which the crack occurred and the point at which the electrical resistance increased were the same. Delamination occurrence points were acoustically detected with the human ear. As the delamination propagations, the contact area decreases and the electrical resistance increases continuously. When a complete fracture occurs, the resistance is greatly increased and the damage of the joint can be monitored.

Polyester(Co-curing)

CFRP

Steel

Figure 33. Schematic diagram of the CFRP-steel single-lap co-cured joints.
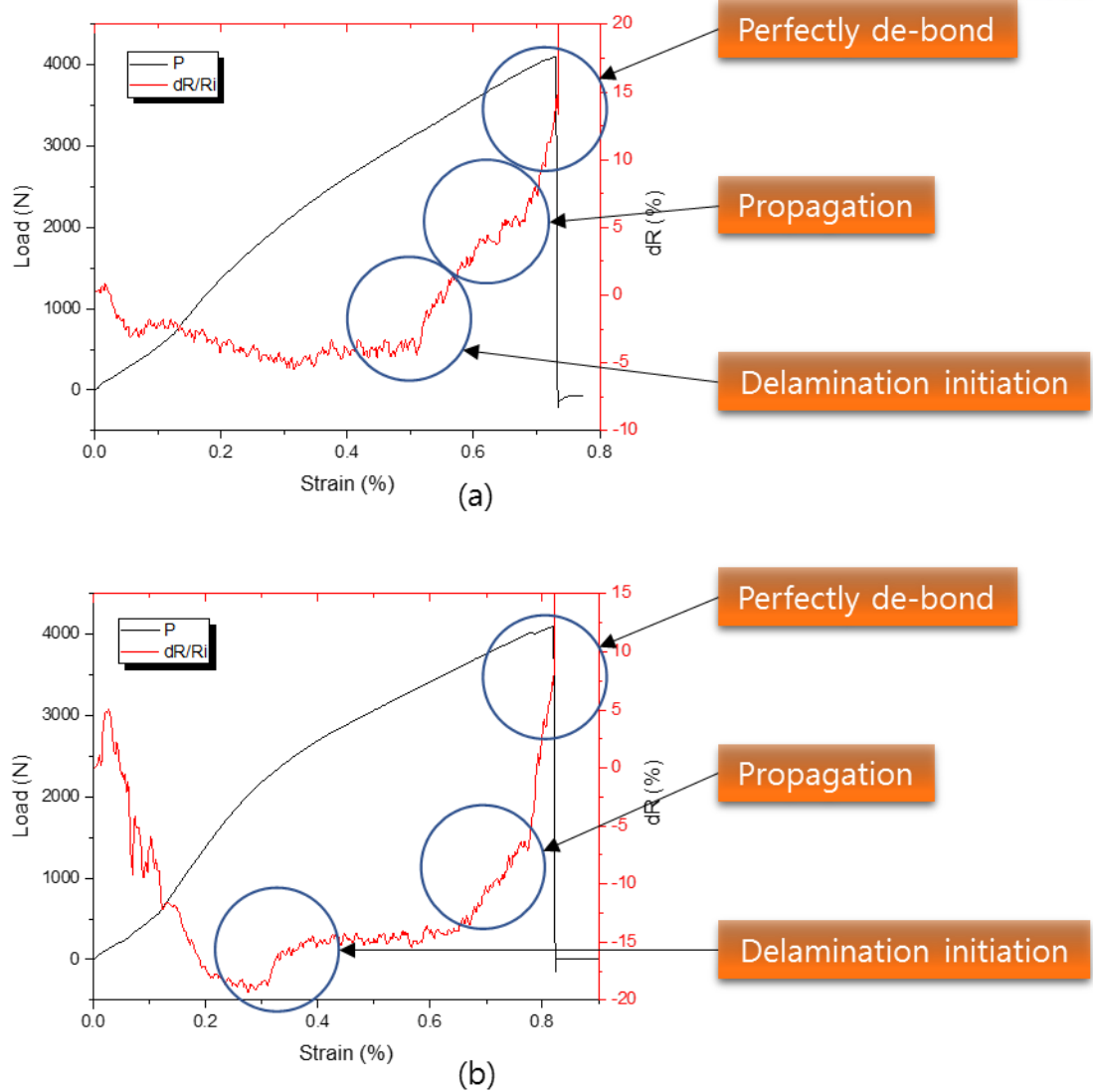
Figure 34. Force and resistance change rate of the CFRP-steel co-cured joints during the test, and crack can be detected using resistance change.

CFRP-aluminum co-cured single-lap joints also have similar electrical resistance changes to multi-material junctions with steel as shown in Fig. 36 (a) and (b). As delamination propagate, the electrical resistance begins to increase and the resistance increases steadily as the crack grows. As a result, it is confirmed that the SHM of the joint is possible by using electrical resistance when the two types of materials such as steel and aluminum which have conductance are joined by co-curing.

Figure 35. Schematic diagram of the CFRP-aluminum single-lap co-cured joints.
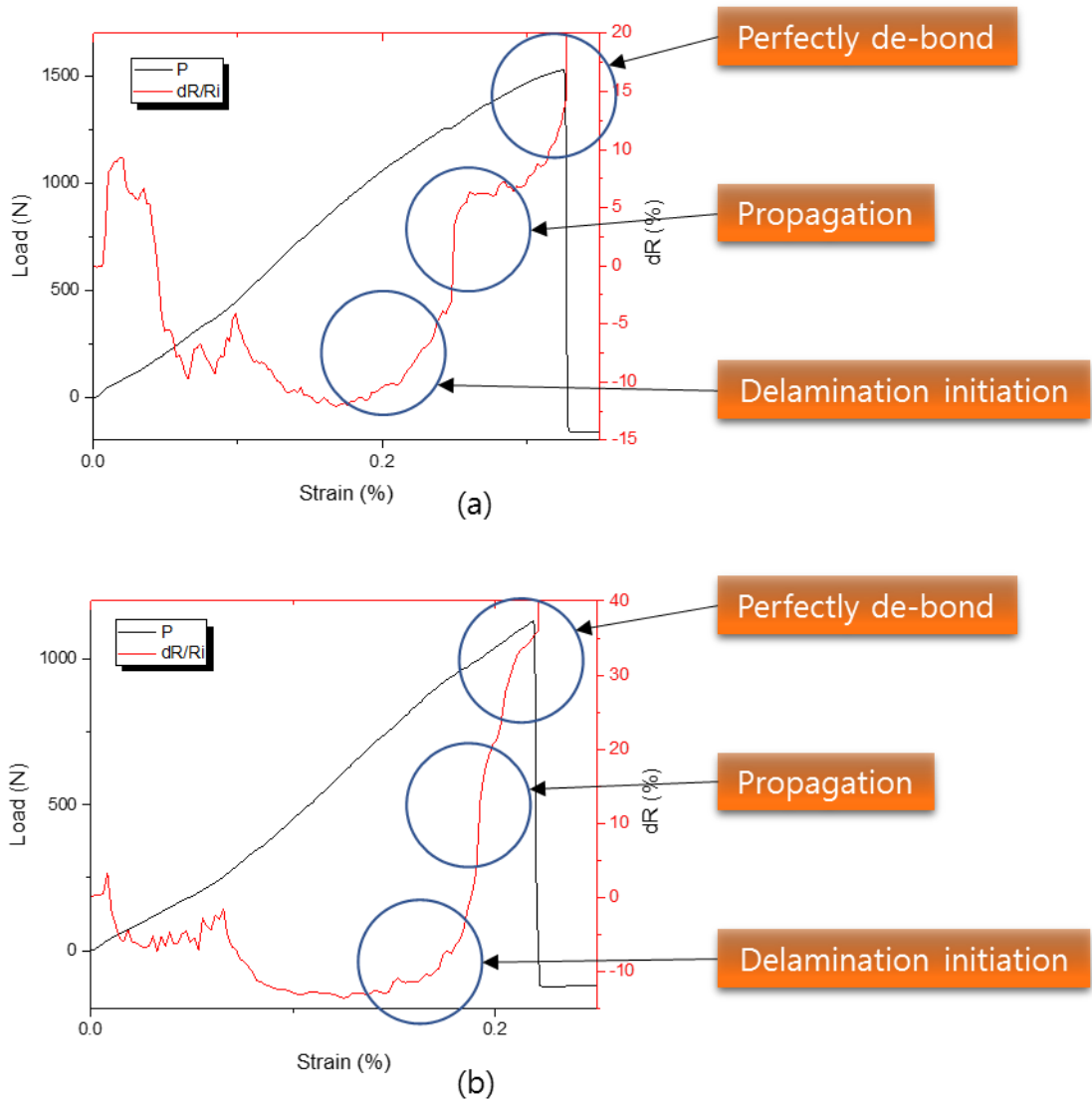
Figure 36. Force and resistance change rate of the CFRP-aluminum co-cured joints during the test, and crack can be detected using resistance change.

For CFRP-CFRP co-cured single-lap joints, the results are shown in Fig. 38. As the tensile strength increases, the electrical resistance decreases, but the electrical resistance before fracture tends to increase gradually. Co-cured joints exhibit increased resistance prior to fracture, either in

multi-material joints with metals or CFRP and same-material joints with CFRPs. This is the main reason for the direct contact between CFRP and metal or CFRP. However, since the joining with metal is a different material, they have different physical properties, so that the carbon fiber and the metal are surely detached when cracking occurs. Therefore, it is possible to clearly distinguish through resistance. However, the bonding between CFRPs is the same material. When the cracks occur due to the cracks, fibers are connected to each other due to textile characteristics, and the slope of the resistance change is low. Figure 39 (c) and (d) show the fractured surface of CFRP-steel co-cured joints, steel and CFRP side, respectively. Figure 39 (e) and (f) show the fractured surface of CFRP-aluminum co-cured joints. Some carbon fibers were stuck on the metal surfaces and broken carbon fiber is not observed as compared to the CFRP-CFRP co-cured joints as shown in Fig. 39 (g). Therefore, the resistance increase of CFRP-CFRP co-cured joints is less than that of CFRP-metal co-cured joints.

Figure 37. Schematic diagram of the CFRP-CFRP single-lap co-cured joints.
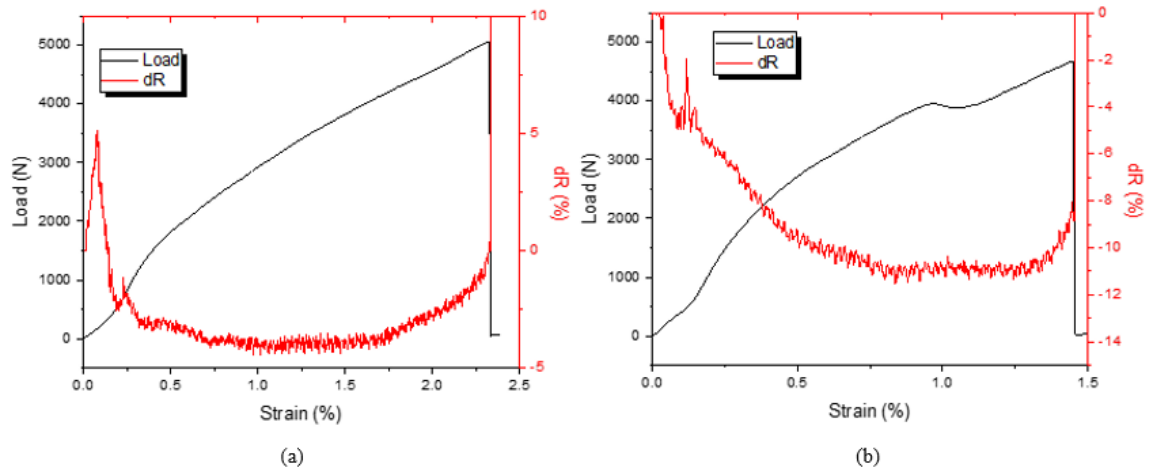
Figure 38. Force and resistance change rate of the CFRP-CFRP co-cured joints during the test.
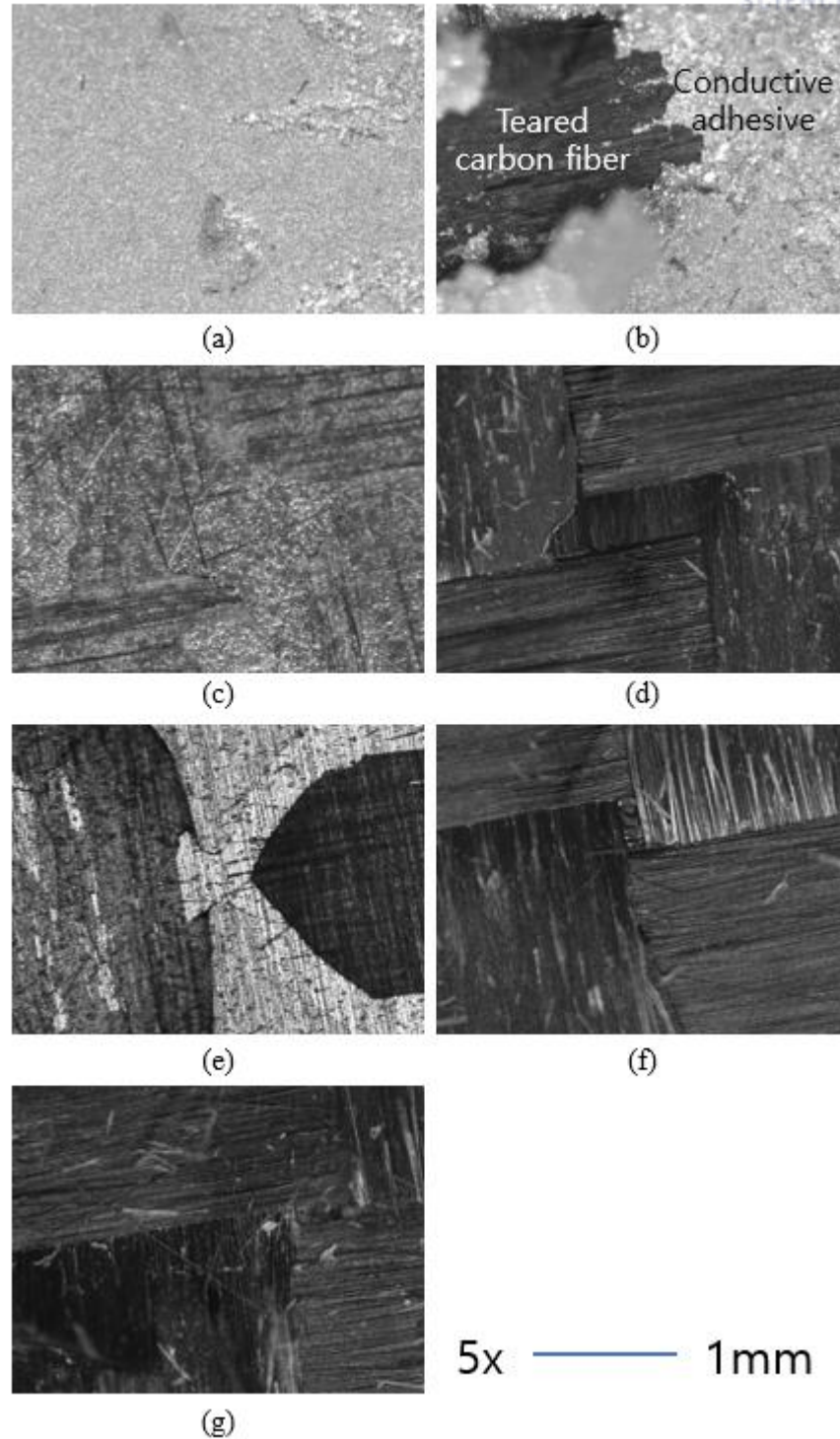
Figure 39. Fractured surface of the single-lap joints from OM with 5 magnified; (a) conductive adhesive, (b) conductive adhesive and teared carbon fiber, (c) steel side surface, (d) CFRP side joined with steel, (e) aluminum side, (f) CFRP side with aluminum and (g) CFRP side from CFRP-CFRP joints.

41

Electrical resistance tends to decrease when load is applied until cracks occur in all samples. This difference is not due to the joining method but is the result of the characteristics of CFRP. CFRP is composed of layered carbon fiber, and each layer is not perfectly aligned. Thus, when CFRP is subjected to tension, the alignment of carbon fibers in each layer increases. As a result, the conductivity of CFRP is increased and the electrical resistance is decreased [42].

4.3.4. Influence of Plasma Treatment on Resistance Change

Co-cured single-lap joints were plasma-treated to enhance the adhesive strength. Therefore, the slope of the resistance change rate before fracture and the adhesive strength were compared in order to confirm how the plasma treatment affects the electrical resistance change in the joint. Figure 40 shows the results. Both steel and aluminum tend to have a decreasing slope before fracture as adhesive strength increases. The change of the electrical resistance in the joint is caused by the area of adhesion. The stronger the adhesive strength is, the faster the breakage occurs, and the smaller the increase in resistance before fracture at the joints.
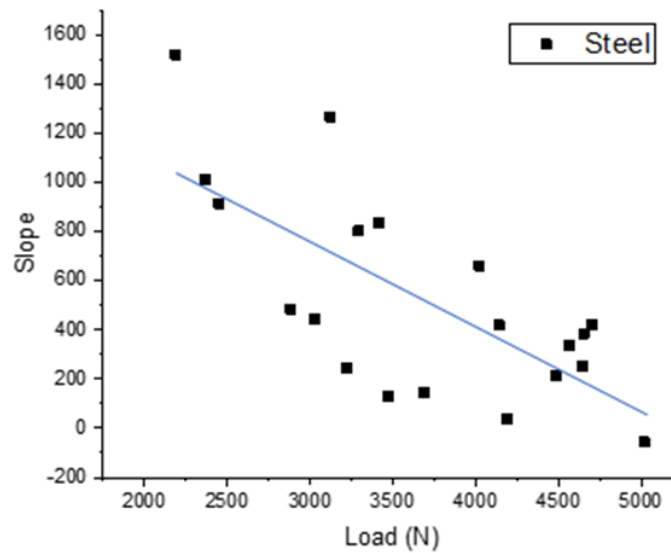
(a)
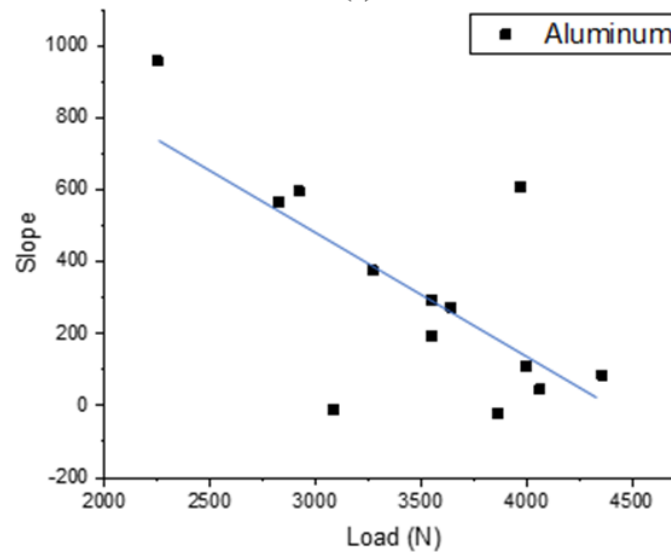
(b)

Figure 40. Resistance change slope before the joints failure and fractured force relationship; (a) Steel and (b) Aluminum.

4.4. Summary

Single-lap joints and bushing-inserted CFRP were fabricated to verify the SHM of joints using electrical resistance. The samples joined by co-curing which were polyester as a matrix or CW 2400 as a conductive adhesive. When the 2-probe method is used for resistance measurement, initial resistance value becomes high due to contact resistance, and it was not possible to capture signs of junction failure by monitoring the resistance change. Therefore, the initial resistance value was decreased by using the 4-probe method, which is not greatly influenced by the contact resistance value, and the resistance variation width was increased in the experiment. Because of the difference in the bonding structure between the co-curing and the conductive adhesive, there is also a difference in resistance variation. Joints bonded with a conductive adhesive showed little or no increase in resistance before fracture. However, the joints bonded by co-curing tended to increase resistance as the contact area of carbon fiber and metal decreased as the fracture occurred. This tendency is gradually reduced as the adhesive strength increases, because the breakage is rapidly generated when the adhesive strength is increased since the section where the resistance increases is reduced. Also, if this result is further developed, it will be possible to predict the joint failure and warn that the breakage at the joints is impending when the slope of the resistance change rate is above a certain threshold value.

5. Conclusions and Recommendations for Future Work

5.1. Conclusions

The use of CFRPs in industry is rapidly increasing, especially in the automotive industry, due their huge potential for lightweighting metal parts and structures. Naturally, as it is practically unrealistic to build a multi-component system entirely consisting of CFRP parts, multi-material joining of CFRP and metal is being studied extensively. Among them, co-curing, in which the matrix of the CFRP is used as the adhesive, and joining is done during the composite manufacturing process, has been proposed as an efficient yet cost-effective way for multi-material joining. In addition, it was demonstrated that the structural integrity of the joints can be monitored by measuring the electrical resistance through the joints real-time.

In Chapter 3, the adhesive strength of single-lap joints fabricated by co-curing and the conductive adhesive were compared, and it was confirmed that co-curing had sufficient adhesive strength. The adhesive strength between aluminum and CFRP was under 1500N, but the strength could be improved by up to 300% by plasma treatment of aluminum surfaces. In the case of steel bushings, the shear strength of bushing and CFRP jointed by co-curing was measured by push-out tests. The shear strength before plasma treatment was about 19MPa, but shear strength was enhanced to 21MPa after plasma treatment. The increase in shear strength is not significant compared to single-lap joints because the contact area between CFRP and bushings is significantly smaller than that of single-lap joints.

In Chapter 4, we verified the feasibility of SHM of various joints by measuring the change in electrical resistance. In the case of joints bonded with a conductive adhesive, which is a conductor, it was difficult to detect joint failures due to cracks. However, in the case of co-cured joints, the initiation and propagation of the cracks can be monitored by the electrical resistance measurements due to the reduction of the contact area because CFRP and metal are in direct contact with each other.

As a result, it was possible to detect the initiation and growth of cracks, as well as failures in co-cured multi-material joints by measuring the electrical resistance. Monitoring of the slope of the change in electrical resistance before fracture in the joint enables fracture prediction. However, there is a trade-off that the sensitivity becomes lower as the adhesive strength becomes higher. We can obtain the co-cured multi-material joints that allows failure prediction if an optimal adhesive strength is identified and if the point where the rate of change in electrical resistance changes corresponding to the fracture point can be found.

5.2.   Future work

   In this experiment, we confirmed that SHM of co-cured multi-materials joints is possible by monitoring the electrical resistance. The biggest challenge left is to identify the changes in stress distribution through simulations of single-lap joints and bushing-inserted CFRPs through finite element analyses and to confirm the current flow by simulation. Finally, based on the experimental and numerical work, it is necessary to establish the criteria for the failure prediction and develop a predictive model.

References

1.   Katayama S, Kawahito Y. Laser Direct Joining between Al. alloy and Plastic or CFRP. Journal of Light Metal Welding. 2013;51(51-12):463-8.

2.   Katayama S, Kawahito Y, Niwa Y, Tange A, Kubota S. Laser direct joining between stainless steel and amorphous polyamide plastic. QJ Jpn Weld Soc. 2007:25-2.

3.   Ueda S. Instantaneous Mechanical Joining between CFRP and Metal. Jnl of Welding Technology. 2015;63(63-4):118-21.

4.   Ratanathavorn W, Melander A. Dissimilar joining between aluminium alloy (AA 6111) and thermoplastics using friction stir welding. Science and technology of welding and joining. 2015;20(3):222-8.

5.   Hoseinlaghab S, Mirjavadi SS, Sadeghian N, Jalili I, Azarbarmas M, Givi MKB. Influences of welding parameters on the quality and creep properties of friction stir welded polyethylene plates. Materials & Design. 2015;67:369-78.

6.   Murr L, Liu G, McClure J. A TEM study of precipitation and related microstructures in friction-stir-welded 6061 aluminium. Journal of Materials Science. 1998;33(5):1243-51.

7.   Gude M, Hufenbach W, Kupfer R, Freund A, Vogel C. Development of novel form-locked joints for textile reinforced thermoplastices and metallic components. Journal of Materials Processing Technology. 2015;216:140-5.

8.   Lambiase F, Di Ilio A. Mechanical clinching of metal–polymer joints. Journal of Materials Processing Technology. 2015;215:12-9.

9.   Lee C-J, Lee J-M, Ryu H-Y, Lee K-H, Kim B-M, Ko D-C. Design of hole-clinching process for joining of dissimilar materials–Al6061-T4 alloy with DP780 steel, hot-pressed 22MnB5 steel, and carbon fiber reinforced plastic. Journal of Materials Processing Technology. 2014;214(10):2169-78.

10.   Abe Y, Kato T, Matsuda A, Mori K-I. Mechanical Clinching of High Strength Steel and Aluminum Alloy A 5052 Sheets. Journal of the Japan Society for Technology of Plasticity. 2010;51(589):141-5.

11.   Balle F, Wagner G, Eifler D. Ultrasonic metal welding of aluminium sheets to carbon fibre reinforced thermoplastic composites. Advanced Engineering Materials. 2009;11(1-2):35-9.

12.   Balle F, Wagner G, Eifler D. Joining of Aluminum 5754 Alloy to carbon fiber reinforced polymers (CFRP) by ultrasonic welding. Aluminum Alloys. 2009:191-6.

13.   Lawcock G, Ye L, Mai Y-W, Sun C-T. The effect of adhesive bonding between aluminum and composite prepreg on the mechanical properties of carbon-fiber-reinforced metal laminates. Composites Science and Technology. 1997;57(1):35-45.

14.   Kim HS, Lee SJ. Development of a strength model for the cocured stepped lap joints under tensile loading. Composite Structures. 1995;32(1-4):593-600.

15.   Huang C. Study on co-cured composite panels with blade-shaped stiffeners. Composites Part A: applied science and manufacturing. 2003;34(5):403-10.

16.   Shin KC, Lim JO, Lee JJ. The manufacturing process of co-cured single and double lap joints and evaluation of the load-bearing capacities of co-cured joints. Journal of materials processing technology. 2003;138(1):89-96.

17.   Kim HS, Park SW. Smart cure cycle with cooling and reheating for co-cure bonded steel/carbon epoxy composite hybrid structures for reducing thermal residual stress. Composites Part A: Applied Science and Manufacturing. 2006;37(10):1708-21.

18.   Olivier P, Cottu J. Optimisation of the co-curing of two different composites with the aim of minimising residual curing stress levels. Composites science and technology. 1998;58(5):645-51.

19.   Park SW, Kim HS. Optimum design of the co-cured double lap joint composed of aluminum and carbon epoxy composite. Composite structures. 2006;75(1):289-97.

20.   Kang M-H, Choi J-H, Kweon J-H. Fatigue life evaluation and crack detection of the adhesive joint with carbon nanotubes. Composite Structures. 2014;108:417-22.

21.   Lange R, Mook G. Structural analysis of CFRP using eddy current methods. NDT & E International. 1994;27(5):241-8.

22.   Riegert G, Zweschper T, Busse G. Lockin thermography with eddy current excitation. Quantitative InfraRed Thermography Journal. 2004;1(1):21-32.

23.   Schulze MH, Heuer H, Küttner M, Meyendorf N. High-resolution eddy current sensor system for quality assessment of carbon fiber materials. Microsystem technologies. 2010;16(5):791-7.

24.   Yin W, Withers PJ, Sharma U, Peyton AJ. Noncontact characterization of carbon-fiber-reinforced plastics using multifrequency eddy current sensors. IEEE Transactions on Instrumentation and Measurement. 2009;58(3):738-43.

25.   Gao D, Wang Y, Wu Z, Rahim G, Bai S. Design of a sensor network for structural health monitoring of a full-scale composite horizontal tail. Smart Materials and Structures. 2014;23(5):055011.

26.   Tsao C. Thrust force and delamination of core-saw drill during drilling of carbon fiber reinforced plastics (CFRP). The International Journal of Advanced Manufacturing Technology. 2008;37(1):23-8.

27.   Soutis C, Curtis P. Prediction of the post-impact compressive strength of CFRP laminated composites. Composites Science and Technology. 1996;56(6):677-84.

28.   Takeda S, Minakuchi S, Okabe Y, Takeda N. Delamination monitoring of laminated composites subjected to low-velocity impact using small-diameter FBG sensors. Composites Part A: Applied Science and Manufacturing. 2005;36(7):903-8.

29.   Botsev Y, Arad E, Tur M, Kressel I, Ben-Simon U, Gali S, et al., editors. Damage detection under a composite patch using an embedded PZT-FBG ultrasonic sensor array. Third European Workshop on Optical Fibre Sensors; 2007: International Society for Optics and Photonics.

30.   Minakuchi S, Banshoya H, Ii S, Takeda N. Hierarchical fiber-optic delamination detection system for carbon fiber reinforced plastic structures. Smart Materials and Structures. 2012;21(10):105008.

31.   Davis CE, Norman P, Ratcliffe C, Crane R. Broad area damage detection in composites using fibre Bragg grating arrays. Structural Health Monitoring. 2012;11(6):724-32.

32.   Davis C, Baker W, Moss SD, Galea SC, Jones R, editors. In situ health monitoring of bonded composite repairs using a novel fiber Bragg grating sensing arrangement. SPIE's International Symposium on Smart Materials, Nano-, and Micro-Smart Systems; 2002: International Society for Optics and Photonics.

33.   Ashby M, Gibson L, Wegst U, Olive R, editors. The mechanical properties of natural materials. I. Material property charts. Proceedings of the Royal Society of London A: Mathematical, Physical and Engineering Sciences; 1995: The Royal Society.

34.   Mallick PK. Fiber-reinforced composites: materials, manufacturing, and design: CRC press; 2007.

35.   Vinson JR, Sierakowski RL. The behavior of structures composed of composite materials: Springer Science & Business Media; 2012.

36.   Wang S, Chung D. Piezoresistivity in continuous carbon fiber polymer-matrix composite. Polymer Composites. 2000;21(1):13-9.

37.   Wang S, Kowalik DP, Chung D. Self-sensing attained in carbon-fiber–polymer-matrix structural composites by using the interlaminar interface as a sensor. Smart materials and structures. 2004;13(3):570.

38.   Takeda T, Shindo Y, Fukuzaki T, Narita F. Short beam interlaminar shear behavior and electrical resistance-based damage self-sensing of woven carbon/epoxy composite laminates in a cryogenic environment. Journal of Composite Materials. 2014;48(1):119-28.

39.   Abry J, Choi Y, Chateauminois A, Dalloz B, Giraud G, Salvia M. In-situ monitoring of damage in CFRP laminates by means of AC and DC measurements. Composites Science and Technology. 2001;61(6):855-64.

40.   Song D-Y, Takeda N, Kitano A. Correlation between mechanical damage behavior and electrical resistance change in CFRP composites as a health monitoring sensor. Materials Science and Engineering: A. 2007;456(1):286-91.

41.   Todoroki A, Yoshida J. Electrical resistance change of unidirectional CFRP due to applied load. JSME International Journal Series A Solid Mechanics and Material Engineering. 2004;47(3):357-64.

42.   Todoroki A, Samejima Y, Hirano Y, Matsuzaki R. Piezoresistivity of unidirectional carbon/epoxy composites for multiaxial loading. Composites Science and Technology. 2009;69(11):1841-6.

43.   Todoroki A. Electric current analysis for thick laminated CFRP composites. Transactions of the Japan Society for Aeronautical and Space Sciences. 2012;55(4):237-43.

44.   Todoroki A, Yoshida J. Apparent negative piezoresistivity of single-ply CFRP due to poor electrical contact of four-probe method. measurement. 2005;1:1-6.

45.   Hibbett, Karlsson, Sorensen. ABAQUS/standard: User's Manual: Hibbitt, Karlsson & Sorensen; 1998.

46.   Kim M, Song D, Shin H, Baeg S-H, Kim G, Boo J-H, et al. Surface modification for hydrophilic property of stainless steel treated by atmospheric-pressure plasma jet. Surface and Coatings Technology. 2003;171(1):312-6.

47.   Murayama H, Kageyama K, Naruse H, Shimada A, Uzawa K. Application of fiber-optic distributed sensors to health monitoring for full-scale composite structures. Journal of Intelligent Material Systems and Structures. 2003;14(1):3-13.

48.   Giurgiutiu V. Tuned Lamb wave excitation and detection with piezoelectric wafer active sensors for structural health monitoring. Journal of intelligent material systems and structures. 2005;16(4):291-305.

49.   Kwon JW, Chin WS, Lee DG. In situ cure monitoring of adhesively bonded joints by dielectrometry. Journal of adhesion science and technology. 2003;17(16):2111-30.

50.   Kim Y, Park K-Y, Kwak S-B. Mechanical fastening and joining technologies to using multi mixed materials of car body. Journal of Welding and Joining. 2015;33(3):12-8.

51.   Tang S, Kwon O-J, Lu N, Choi H-S. Surface characteristics of AISI 304L stainless steel after an atmospheric pressure plasma treatment. Surface and Coatings Technology. 2005;195(2):298-306.

52.   Suzuki M, Kishida A, Iwata H, Ikada Y. Graft copolymerization of acrylamide onto a polyethylene surface pretreated with glow discharge. Macromolecules. 1986;19(7):1804-8.

53.   Ito Y, Inaba M, Chung DJ, Imanishi Y. Control of water permeation by pH and ionic strength through a porous membrane having poly (carboxylic acid) surface-grafted. Macromolecules. 1992;25(26):7313-6.

Acknowledgements